Robust Composite Controller for Stability Enhancement in Hybrid AC/DC Microgrids Incorporating Renewable Hydrogen Storage.



SONARGAON UNIVERSITY (SU)

Submitted By

Md. Zubair Hossain Shanto	**ID: EEE2102023009**
Swapan Barai	**ID: EEE2103024002**
Sumon Hossain	**ID: EEE2101022014**
Md. Imran hossen	**ID: EEE2103024101**
Rony Mia	**ID: EEE2103024027**

Supervised By
Md. Saiful Islam
Lecturer Department of EEE
Sonargaon University (SU)
147/I, Green Road, Tejgaon, Dhaka-1215

Declaration

We declare that this thesis paper, titled *"***Robust Composite Controller for Stability Enhancement in Hybrid AC/DC Microgrids Incorporating Renewable Hydrogen Storage***"*, is our own work and has not been submitted to any other institution or university for the award of any degree or diploma. All the sources we used in this thesis have been properly cited and acknowledged. We understand the importance of honesty in academic work and confirm that this thesis follows the rules of academic integrity.

_____ _____

Zubair Hossain Shanto **Swapan Barai**

_____ _____

Sumon Hossain **Md. Imran hossen**

_____

Rony Mia

Under Supervision of

_____

Md. Saiful Islam

Lecturer, Department of Electrical and Electronics Engineering (EEE)

Sonargaon University (SU)

Certification

This is to certify that this project entitled "**Robust Composite Controller for Stability Enhancement in Hybrid AC/DC Microgrids Incorporating Renewable Hydrogen Storage**" is done by the following students under my direct supervision. This project work has been carried out by them in the laboratories of the Department of Electrical and Electronics Engineering under the Faculty of Engineering, Sonargaon University (SU) in partial fulfillment of the requirements for the degree of Bachelor of Science in Electrical and Electronics Engineering.

Supervisor

_____

Md. Saiful Islam

Lecturer, Department of Electrical and Electronics Engineering (EEE)

Sonargaon University (SU)

Acknowledgement

We are deeply grateful to our respected supervisor, Md. Saiful Islam, Lecturer, Department of Electrical and Electronics Engineering, Sonargaon University, for his continuous guidance, support, and insightful feedback throughout the completion of this undergraduate thesis titled “Robust Composite Controller for Stability Enhancement in Hybrid AC/DC Microgrids Incorporating Renewable Hydrogen Storage.” His profound knowledge, encouragement, and commitment to high academic standards were instrumental in every phase of this research.

This research represents the collaborative effort of a dedicated group of five students: Zubair Hossain Shanto, Swapan Barai, Sumon Hossain, Md. Imran Hossen, and Rony Mia. Each member of this team contributed significantly to the successful execution and completion of the project, bringing individual strengths, technical skills, and analytical rigor to every stage of the work.

We would also like to thank the Department of Electrical and Electronics Engineering, Sonargaon University, for providing a conducive academic environment and the necessary laboratory and computational facilities which enabled the simulation, modeling, and evaluation of our proposed control strategy. We extend our special thanks to Prof. Shamim Ara Hassan, Honorable Vice Chancellor of Sonargaon University, and Md. Rais Uddin Mollah, Assistant Professor & Head (Acting), Department of Electrical and Electronics Engineering, for their invaluable support and encouragement throughout our academic journey.

The completion of this thesis marks a significant milestone in our academic journey, one that would not have been possible without a combination of team effort, scholarly mentorship, and institutional support. We sincerely acknowledge all the individuals who, directly or indirectly, contributed to the successful realization of this research work.

Abstract

The growing adoption of renewable energy sources and the development of hybrid AC/DC microgrid architectures have significantly improved the flexibility, reliability, and energy efficiency of modern power systems. These microgrids are particularly valuable in distributed generation environments, where diverse energy sources like solar, wind, battery storage, and hydrogen systems are integrated. However, maintaining stable operation and controlling power flow within these systems remains a key technical challenge due to the intermittent nature of renewable energy and the complex dynamics between AC and DC subsystems. In this thesis, we propose a robust composite control strategy that combines terminal sliding mode controller (TSMC) with backstepping controller (BSC). This approach, known as terminal sliding mode backstepping controller (TSMBC), is designed to enhance system stability, improve dynamic response, and maintain voltage regulation under varying load and generation conditions. To assess its effectiveness, the proposed TSMBC controller is compared with an existing method, the existing double integral sliding mode controller (EDISMC), through detailed simulations carried out in MATLAB/Simulink. The simulation results clearly demonstrate that TSMBC offers superior performance across several important metrics. Specifically, TSMBC achieved up to 100% reduction in overshoot and up to 99% improvement in settling time, resulting in significantly faster stabilization and enhanced transient response in most scenarios. In contrast, the existing EDISMC controller often exhibited delayed response and higher overshoot values. These improvements were consistent across a wide range of components, including photovoltaic (PV) units, permanent magnet synchronous generators (PMSGs), battery energy storage systems (BESS), DC/AC loads, electrolyzer, PEM fuel cell and hydrogen storage systems. Overall, the proposed control strategy proves to be more effective, adaptive, and resilient, supporting stable operation even under fluctuating power conditions.

Table of Contents

Topics	Page No
Declaration	ii
Certification	iii
Acknowledgement	Iv
Abstract	V
Table of Contents	vi
Nomenclature & Symbol	vii-viii
CHAPTER 1: INTRODUCTION	01
1.1 Background and challenges	01
1.2 Literature review	02-05
1.3 Research gaps	05-07
1.4 Motivation and contribution	08
CHAPTER 2: OPERATING PRINCIPLES AND CONFIGURATION OF HADMG	09
2.1 System Configuration	09
2.2 Principles of Operation	09-10
CHAPTER 3: DYNAMICAL MODEL OF HYBRID AC/DC MICROGRID	11
3.1 Modeling of BVSC with an LC filter	11
3.2 Modelling of a solar PV unit with a DDBC interface	11-12
3.3 Modeling of a PMSG unit with a DDBC interface	12-13
3.4 Modeling of a BESS unit with a BDDC interface	14
3.5 DDBC numerical modeling using a PEMFC	14-15
3.6 Electrolyzer modeling using a DC-DC buck converter	15
CHAPTER 4: THE SUGGESTED DESIGN FOR THE CONTROLLER	16
4.1 Design of the TSMBC for the BVSC	16-21
4.2 Design of the PV's TSMBC in combination with a DDBC	21
4.3 Combining a rectifier for a PMSG with a TSMBC design for the DDBC.	21
4.4 Together with the BESS, the TSMBC design for the BDDC.	22
CHAPTER 5: PERFORMANCE EVALUATION OF THE CONTROLLER	23
5.1 Selection of simulation parameters	23-24
5.2 Implementation block diagram	25

5.3 Simulation results	25-33
5.4. Discussion	34
CHAPTER 6: CONCLUSION	35-35
REFERENCES	37-41

Nomenclature & Symbol

List of abbreviations and full forms:

ANN	Artificial Neural Network
BSC	Backstepping Controller
BDDC	Bidirectional DC–DC Converter
BESS	Battery Energy Storage System
BVSC	Bidirectional Voltage Source Converter
DDBC	DC–DC Boost Converter
DDT-MPC	Data-Driven Tuning-based Model Predictive Control
DG	Distributed Generation
FBL	Feedback Linearization
FRSMC	Fast Reaching Sliding Mode Control
FTBSC	Finite-Time Backstepping Sliding Mode Control
GITSMC	Generalized Integral Terminal Sliding Mode Control
GRESs	Green Renewable Energy Sources
HADMG	Hybrid AC/DC Microgrid
ITSMC	Integral Terminal Sliding Mode Control
MG	Microgrid
MPC	Model Predictive Control
NFTSMC	Nonlinear Fast Terminal Sliding Mode Control
PEMFCs	Proton Exchange Membrane Fuel Cells
PI	Proportional–Integral
PID	Proportional Integral Derivative
PV	Photovoltaic
SG	Synchronous Generator
SMC	Sliding Mode Controller
TSMBC	Terminal Sliding Mode Backstepping Controller

List of symbols and full forms:

$P_{AC-load}$	Solar PV Power
P_{BESS}	Power of a Battery
$P_{DC-load}$	DC-load Power
P_{loss}	Power Loss of a System

P_{pv}	Solar PV Power
P_{wind}	Wind Power
C_{dc}	DC-bus Capacitance
C_f	Filter Capacitor
I_{id}	Input Current of a BVSC in d-axis
I_{iq}	Input Current of a BVSC in q-axis
I_{od}	Output Current of a BVSC in d-axis
I_{oq}	Output Current of a BVSC in q-axis
L_b	Converter's Inductance of a Battery System
L_f	Filter Inductor
M_d	Control Input for a BVSC in d-axis
M_q	Control Input for a BVSC in q-axis
R_b	Converter's Internal Resistance of a Battery
S_oC	State of Charge of a Battery
V_{cd}	Voltage of a Capacitor in d-axis
V_{dc}	DC-bus Voltage DC-bus Voltage
V_{cq}	Voltage of a Capacitor in q-axis
ω	Angular Frequency

Chapter 1
Introduction

1.1 . Background and challenges

Fossil fuels and traditional power plants are being increasingly displaced by renewable energy sources (RESs) due to the growing global demand for electricity, the adverse environmental effects of burning fossil fuels, and the diminishing reserves of oil resources [1–3]. The reliance on fossil fuels has also highlighted the negative impacts of synchronous generators, including their significant contribution to greenhouse gas emissions and environmental degradation. Over the last two decades, the concept of distributed generation technologies has emerged as a transformative force, facilitating the transition from conventional power generation to sustainable energy generation with support from various stakeholders [4]. Solar photovoltaic (PV) and wind systems, which produce abundant and renewable energy, play a pivotal role in enhancing carbon durability and reducing the dependence on fossil fuel-based power systems. However, the widespread adoption of RES introduces challenges in balancing demand and generation within the distribution system due to their inherently variable and unpredictable nature. The integration of RESs and energy storage systems has been significantly optimized with the introduction of the microgrid (MG) concept [5, 6]. MGs offer several advantages, including enhanced autonomy, improved reliability, flexibility in meeting load demands, and superior stability in both grid-connected and islanded modes. These features make MGs indispensable for achieving a more resilient and sustainable energy infrastructure [7, 8].

In various applications, DC power generated by PV units and battery storage systems can be directly utilized to meet DC load requirements. This approach offers a simplified control mechanism compared to AC systems, as it eliminates the need for frequency regulation and reactive power management [9,10]. Moreover, rectifier conversion circuits are unnecessary when using RESs that produce AC power to supply AC loads directly. The scientific community has therefore paid close attention to hybrid systems with renewables in recent decades [11], as they combine the benefits of both DC and AC microgrids [12].These systems can efficiently manage DC and AC loads without requiring additional conversions between DC and AC, thereby reducing conversion losses and improving energy efficiency. A critical feature of hybrid microgrids is the interplay between DC and AC systems via a bidirectional voltage source converter (BVSC), which simplifies power conversion processes while enhancing system stability and control operations [13]. However, despite their advantages, microgrids face several challenges, primarily due to variations in load demand and the intermittency of RESs [14]. The most prevalent RESs in an MG are known to be wind generators and photovoltaic units, whose output power is dependent on wind velocity and irradiance. Furthermore, because it is used to balance out RES swings by storing excess energy and releasing it based on load conditions, the BESS has emerged as a crucial part of microgrids. In addition, a typical hybrid microgrid consists of four key parts: power electronic grid interfaces, load, BESSs, and generating systems [15]. For an MG to operate dependably and economically during power system emergencies, the ideal power flow between these parts is necessary to maintain the stability of the DC bus and AC bus voltages at the appropriate levels. Furthermore, it is crucial to improve the stability of the DC bus voltage in order to provide the best possible power flow on both the DC-side and the AC-side of hybrid systems. For hybrid AC-DC microgrids (HADMGs) to improve stability while ensuring resilience against these circumstances, controllers are therefore required.

1.2. Literature review

Studies in [16–18] highlight the use of linear control strategies to enhance AC voltage and DC bus stability while managing power flow in individual AC and DC microgrids. A model-free proportional-integral (PI) control system, as proposed in [19,20], coordinates the actions of controllers linked to specific microgrid components to regulate power effectively. PI controllers, however, cannot guarantee the HADMG's stability over a range of operating conditions. A system with a similar control method was put forth in [21], where the controller is made especially to manage frequency and voltage for an induction wound rotor generator, with less focus on managing other parts of the same MG. In [22], a BWOA-PIDF-(1+I) controller is introduced to lessen the impact of the demand-generation discrepancy and the change in frequency deviation. However, only a stand-alone system can use the suggested control approach.

In a prior work [23], parallel bidirectional power flow converters were integrated into a system using a distributed control system. Nevertheless, the stability issues related to both AC and DC bus voltages were disregarded by the controllers used in [23]. Furthermore, a major disadvantage of linear controllers is their incapacity to guarantee the hybrid microgrid's worldwide stability in a variety of operating scenarios, such as an abrupt loss of a sizable amount of generation or a large load demand. This is due to the fact that a linear controller can only offer small signal stability around a single operating point and depends on linear small-signal models of the managed system. In [24], a nonlinear perturbation observer-based microgrid control technique is introduced to reduce this drawback while maintaining system stability in a large signal setting. However, because it is challenging for a disturbance observer to accurately forecast all likely disturbances, the control mechanism in [24] is still reliant on the PI method, which is still susceptible to changes in a HADMG.

In order to get over the aforementioned restrictions, Ref. [25] uses a generalised droop management technique to provide acceptable power sharing and DC bus voltage dynamic stability in a HADMG. It ignores the communication between DC and AC systems, though. In order to overcome this limitation, a different droop controller was put forth in [26] to power the bidirectional VSC's switching signal for power exchange between a HADMG's AC and DC sides. But the stability analysis's rigour isn't assured. Additionally, a significant problem with these droop control systems [27] is that they are vulnerable to voltage variations at the DC and AC microgrid interface points, which are the DC and AC buses, respectively. Furthermore, there is a higher chance of such mistakes in hybrid systems since the droop controller is built using the linearity properties of various MG components. This is due to the fact that RES behavior's intermittency expands the dynamic operating zones for MG operation. Consequently, the dynamic stability of the entire MG is not ensured by the employment of these droop controllers.

The current literature reports a number of nonlinear control strategies for HADMGs to guarantee the stability of the DC bus and AC bus in order to address the aforementioned issues [28, 29]. It is commonly known that nonlinear mathematical models may accurately represent the nonlinear properties of different DC microgrid components. It has also been demonstrated that the dynamic efficiency of the DC microgrid can be significantly increased by using nonlinear mathematical models to build the nonlinear controllers [30, 31]. A model predictive controller (MPC), which optimises the performance index, is suggested in [32] and [33] to lessen the negative nonlinear influence on DC microgrids. Nevertheless, the MPC necessitates more processing time for optimisation, which reduces the controller's effectiveness even further. An enhanced EMS architecture using distributed dynamic tube MPC (DDT-MPC) is presented in [34] to get around this restriction and efficiently handle uncertainty in multi-microgrids with fluctuating demand and RESs. By transforming uncertainty into predictable, optimal scheduling calculations, this method reduces

conservatism and significantly boosts economic efficiency. However, slow dynamics and model errors restrict DDT-MPC's performance. An artificial neural network (ANN)-based MPC strategy is proposed in [35] to address the challenges of DDT-MPCs, ensure DC-bus stability of DC microgrids, and get rid of issues with conventional MPC methods. Even though the ANN-MPC addresses the shortcomings of traditional MPCs, a training data set is still necessary for its operation. Furthermore, the strong performance of the controller is weakened by an erroneous training data set.

A feedback linearisation (FBL) controller is proposed in [36] to address the aforementioned drawbacks by preserving a steady DC-bus voltage and proper power balance inside the DC microgrid. Another flexible FBL controller is introduced in [37] to enhance the DC microgrid's power-sharing capabilities and estimate the unidentified system aspects. However, achieving the required DC-bus voltage tracking effectiveness and quick dynamic responses requires precise system settings. Acquiring precise system parameters in practice is similarly difficult. A backstepping controller (BSC) for DC microgrids is introduced in [38-40] to mitigate this vulnerability. It maintains power balance and guarantees the dynamic stability of the DC-bus voltage over a range of operating regimes. It is susceptible to external disturbances (EDs), though, which are common in DC microgrid operations. Additionally, an adaptive BSC is reported in [41] by greatly enhancing the tracking performance of the DC-bus voltage against PUs. However, since optimal performance cannot be achieved without adequate tuning, optimising adaption settings is essential to attaining the necessary voltage tracking. Furthermore, the DC microgrid was not viable in the suggested system since solar PVs were the only power-generating units, ignoring other RESs. In order to get around this restriction, a DC microgrid with extra RESs, supercapacitors, and battery storage was suggested in [42]. To enable distributed, autonomous power management and preserve steady DC-bus voltage regulation, the system makes use of a finite-time backstepping controller (FTBSC). In order to minimise important disturbances within a given time frame, a finite time disturbance observer is also implemented. Notwithstanding these benefits, the FTBSC presents difficulties for real-world implementation because of its complex control algorithms and requirement for real-time calculation.

As discussed in [43-47], nonlinear sliding mode controllers (SMCs), which are well-known for their ability to tolerate EDs and PUs, offer a viable remedy for the shortcomings of the FBL and BSC approaches. An SMC is described in [48] to control all power converters connected to DC microgrids in order to achieve the best possible power flow between the elements of the MG and the common DC-bus. Although the aforementioned SMC techniques are effective in regulating the DC-bus voltage, chattering in the switching control signals continues to be a problem for them. A fast-response sliding mode control (FRSMC) approach is presented in [49] for PV and wind-based DC microgrids in order to overcome these constraints. To control dual-stage converters in an islanded PV microgrid, a nonsingular fast terminal sliding mode control (NFTSMC) method is also suggested in [50]. By efficiently handling a variety of disruptions, including variations in solar radiation and variations in load demand, the NFTSMC approach improves the system's resilience and guarantees steady and dependable MG operation. A drawback of the aforementioned concept is the lack of ESSs, which are essential components of DC microgrids, even if FRSMC and NFTSMC offer stable dynamics against fluctuating circuit parameters and EDs. A terminal SMC (TSMC) is presented in [51] to overcome this limitation and ensure the transient stability of DC microgrids based on PV, wind, and BESS. However, because neither PUs nor EDs are included in the mathematical modelling of the DC microgrid, the TSMC struggles with rapid transients. To solve the issues in [52], a higher-order SMC with a proportional–integral– derivative (PID)-based sliding surface has been proposed in [53] by taking the EDs into account. Nevertheless, the suggested controller has a considerable degree of DC-bus voltage tracking inaccuracy because of the PID-based sliding surface. In order to reduce the inaccuracy in DC-bus voltage tracking, a double-integral SMC (DISMC) is suggested in [54]. Nevertheless, unanticipated chattering

issues are introduced by the traditional reaching law. To maintain precise power balance and stabilise the DC-bus voltage during fluctuating operating regimes, an improved exponential reaching rule-based SMC approach is employed in [55] for a DC microgrid comprising PV, wind, and dual-energy storage systems. Despite their greater dependability, battery and ultracapacitor-based energy storage make DC microgrid operation and control needlessly more difficult. Additionally, to address the issues raised in [56] and [57], a robust integral terminal SMC (ITSMC) is proposed in [58, 59]. It offers better DC-bus voltage regulation with fewer integral errors, overshoots, and settling times, as well as effective power management in microgrids. The robust ITSMC's primary drawback is that it can only be used with first-order systems, which limits its ability to control one degree of freedom. Because it has a direct impact on the voltage applied to the load, efficient DC-bus voltage regulation is therefore essential. As a result, the ITSMC is insufficient for obtaining the necessary control performance when working with converters that are represented as second-order systems. In order to address the shortcomings of ITSMC, a global integral terminal sliding mode control (GITSMC) approach was presented in [60], guaranteeing both transient and dynamic stability in the face of significant fluctuations in solar irradiation and load demands. Notably, compared to other sophisticated SMC techniques, GITSMC optimises power distribution among PV systems, BESS, and DC loads in addition to controlling the DC-bus voltage. However, the modelling of the DC microgrid does not take into account the model perturbations and EDs. The discussion above makes it abundantly evident that each control approach has pros and cons of its own, which could make it more challenging to reach the necessary degree of control effectiveness.

To get around the previously mentioned restrictions, the composite control methods will be a good option to address the problems related to DC microgrids by leveraging the benefits of multiple control strategies (such as SMCs and BSC). A composite backstepping SMC (BSMC) design was suggested by [61] in order to successfully eliminate the disrupted zero dynamics in DC microgrids and provide overall stability under large-signal situations. The advantages of both traditional SMCs and BSCs are combined in this composite material control approach. In order to properly control the DC bus voltage for a PV, wind, and battery storage-based DC microgrid, one more composite technique is presented in [62]. This durable hybrid controller is built by combining a fractional-order SMC approach with an adaptive an integral backstepping controller. The negative effects of chattering are lessened by these composite material controllers, which also improve their ability to refuse disturbances. Even so, eliminating the chattering from variables switching control signals completely while maintaining high precision in DC microgrid performance remains challenging. As mentioned in [63], a terminal sliding mode backstepping control (TSMBC) approach was used in a number of MG components to overcome the drawbacks and improve stability responses. In a variety of RESs and load scenarios, the composite TSMBC approach performs better. Its overall efficacy is limited, though, as its resilience is diminished by the omission of primary sections and devices for energy from the style procedure. A backstepping global integral terminal sliding mode control (BGITSMC) method is suggested in [64] as a solution to these problems. By successfully stabilizing microgrids and guaranteeing convergence to desirable states, this combined BGITSMC technique presents a viable way to improve system performance. Notwithstanding its benefits, BGITSMC has difficulties in controlling computational complexity, choosing the right gain values, and necessitating accurate system modeling. Furthermore, tertiary power sources like proton exchange the membrane fuel cells (PEMFCs), which are essential for preserving stability during variations in solar and wind generations, are frequently absent from older DC microgrid systems. To control nonlinear interruptions and preserve a steady DC-bus voltage, an interruption observer-based combined BSMC is introduced in [65].The recommended DC microgrid topology, however, only includes a PV system. Furthermore, the DC microgrid has trouble supplying the required amount of electricity to the consumer's end at night or in situations where solar PV

conditions are erratic. In [66], a comparable composite controller for energy converters in DC microgrids that combines BSC and DISMC is proposed. By including a proactive disturbance adjustment mechanism, this novel method effectively mitigates unmodeled uncertainty without requiring an observer. While composite control strategies enhance the stability and performance of DC microgrids, another critical challenge is the issue of inertia, which affects both AC and DC microgrid stability. Addressing this challenge is key to ensuring reliable operation in hybrid microgrids.

1.3. Research gaps

The literature highlights advancements in control strategies for HADMGs. However, several limitations remain, warranting further research to enhance control efficacy, stability, and robustness. The identified gaps are as follows:

- **Limitations of linear control strategies:** Linear methods like PI and PID controllers are widely used for voltage stability and power flow management. While optimization techniques improve robustness, their performance declines in highly nonlinear and uncertain systems. These controllers, optimized for specific conditions, struggle to adapt to the dynamic nature of HADMGs, especially during large disturbances.
- **Challenges with FBL Controllers:** Nonlinear FBL controllers stabilize DC bus voltages and maintain power balance but rely heavily on precise system parameter values. Obtaining such information is often impractical, leading to degraded performance under parametric uncertainties.
- **Vulnerabilities of BSCs:** BSCs enhance dynamic stability and power balance but are sensitive to external disturbances. Additionally, certain BSC designs are confined to specific configurations, such as DC microgrids with PV units and batteries, limiting their applicability in broader hybrid systems.
- **Shortcomings of SMCs:** SMCs are promising for stabilizing HADMGs but suffer from chattering due to conventional reaching laws. Lyapunov-based adaptive controllers and double-integral SMCs (DI-SMCs) address some issues but still face limitations:
    - Lyapunov-based controllers struggle with DC bus voltage tracking accuracy due to single-integral sliding surfaces.
    - DI-SMCs reduce steady-state errors but continue to experience chattering.
- **Challenges in advanced ITSMC:** ITSMC mitigates chattering and improves accuracy but falls short in handling parametric uncertainties and interconnected dynamics, such as load current influences on DC bus voltage.
- **Need for a hybrid control strategy:** The limitations of individual control methods emphasize the need for a hybrid strategy that combines their strengths, ensuring robust, adaptive, and stable performance in diverse operational conditions.
- **Complexity in Composite Control Designs:** Composite controllers—integrating multiple strategies such as BSC, SMC, and adaptive modules—have shown improved stability and robustness. However, these methods suffer from complex tuning procedures, computational burden, and implementation challenges during real-time operation, especially in systems with rapidly varying loads.
- **Hydrogen-Based Storage System Integration Challenges:** Despite the increasing interest in hydrogen energy systems such as PEM fuel cells and electrolyers, most control strategies do not address their dynamic behavior. The absence of hydrogen storage integration in controller design restricts the controller's applicability in low-carbon, long-duration storage microgrids.

- **Observer Dependency and Model Inaccuracy:** Several advanced control approaches (e.g., observer-based SMCs or ANN-based controllers) rely heavily on precise model prediction or training data. Any deviation or mismatch leads to degraded performance and unreliable output in real-time scenarios.
- **Neglect of Coupled AC/DC Dynamics:** Existing control designs frequently treat AC and DC microgrids as separate subsystems. This neglects the complex coupling effects introduced by bidirectional converters, leading to inaccurate control signals, voltage imbalances, and reduced overall system efficiency.

The following table summarizes the key control strategies discussed in the literature, highlighting their main contributions and associated limitations.

Controller	Key Contributions	Limitations	Reference
PI / PID	Widely used for voltage and frequency control; simple to implement.	Ineffective under non-linear, high disturbance environments.	[24]
Droop Control	Supports decentralized power sharing; useful in islanded and grid-connected modes.	Weak voltage regulation; limited AC/DC stability.	[25–27]
MPC	Optimizes multiple objectives with constraints.	Computationally intensive; sensitive to model errors.	[32–34]
DDT-MPC	Improves economic efficiency under uncertainty.	Model errors reduce performance; slow dynamics.	[34]
ANN-MPC	Enhances adaptability and control precision.	Requires large dataset and training; not real-time ready.	[35]
ANN-MPC	Eliminates model dependency; improves tracking.	Needs large, accurate training data set.	[35]
FBL	Ensures voltage regulation via linearization; handles system non-linearity locally.	Highly parameter-dependent; lacks robustness in uncertain environments.	[36–37]
BSC	Improves transient response and dynamic voltage support.	Complex gain tuning; sensitive to disturbances.	[38–41]
FTBSC	Finite-time voltage regulation; enhanced disturbance rejection.	Complex algorithm; requires real-time computation.	[42]
SMC	Robust against parameter variation; good transient tracking.	Chattering issue; reaching law design required.	[43–47]

FRSMC	Fast sliding mode response; improved stability under PV/wind variation.	Chattering and lacks ESS integration.	[49]
NFTSMC	Handles varying irradiance/load; ensures microgrid resilience.	No energy storage system; limited applicability.	[50]
TSMC	Ensures transient stability for PV/Wind/BESS based MGs.	Struggles with fast transients; lacks disturbance modeling.	[51]
DISMC	Enhances robustness; reduces steady-state error.	Residual chattering and switching loss remain.	[54]
ITSMC	Improves response speed and convergence under nonlinearity.	Limited to first-order systems; sensitive to gain settings.	[58–59]
GITSMC	Provides fast convergence; effective under solar/load fluctuation.	Model uncertainties not fully addressed.	[60]
BSMC	Addresses zero dynamics; enhances DC voltage control.	Difficult to tune; potential switching instability.	[61]
FOSMC + Adaptive BSC	Reduces chattering; manages disturbances better.	Highly complex and difficult to implement in real time.	[62]
TSMBC	Improves stability with multiple RES; fast transient recovery.	Neglects some dynamic interactions; tuning complexity.	[63]
BGITSMC	Handles grid fluctuations and hydrogen system dynamics effectively.	High computation cost; model-dependent.	[64]
Observer-Based BSMC	Enhanced performance under uncertainty with PV integration.	Limited scalability; observer design dependent.	[65]
BSC + DISMC	Improves disturbance rejection without observer.	Gain tuning sensitive; limited real-time validation.	[66]
Composite Controller (BSC+SMC) [Current Work]	Combines robustness, disturbance rejection, and voltage stability.	Complex to implement; high computational burden.	[Proposed]

1.4. Motivation and contributions

Hybrid electrical systems comprising diverse energy storage systems (ESSs), distributed generators (DGs), and AC and DC loads pose significant operational challenges, particularly in achieving coordinated control to enhance dynamic stability and transient response. To address these challenges, a more adaptable, accurate, and efficient control strategy is essential to ensure stability under varying load patterns, generation levels, and operating conditions. This study proposes a TSMBC for hybrid AC-DC microgrids (HADMGs) with RESs and battery energy storage systems (BESSs). The proposed control strategy ensures global stability by generating control inputs that drive system states to their desired values within a finite timeframe, providing both transient and dynamic stability across a wide range of operating scenarios. To the best of the author's knowledge, this is the first attempt to apply a composite terminal sliding mode and BSC for HADMG control. The stability of the proposed scheme is analyzed using Lyapunov function theory, and its effectiveness is validated through simulations, outperforming existing enhanced SMC (ESMC) methods, as reported in [80].

Key contributions of this study include:

- **Comprehensive Modeling**: Global dynamic models of key components, including a solar PV unit, BESS, wind generator based on a permanent magnet synchronous generator (PMSG), and BVSC with LC filters, are developed to support the controller design.
- **Enhanced Stability**: The BESS mitigates the impact of solar PV power fluctuations and PMSG variability on both AC and DC loads.
- **Improved Power Sharing**: The proposed controller maintains effective power-sharing among RESs (e.g., PMSG, PV unit) and the BESS during unexpected system events, reducing AC and DC bus voltage fluctuations.
- **Finite-Time Convergence**: Control inputs are designed using Lyapunov stability analysis to ensure monitoring errors converge to zero within a finite time while maintaining global HADMG stability.
- **Superior Performance**: Simulation results confirm the composite controller's superior performance compared to existing methods under various operating scenarios.

This study provides a robust and innovative solution for improving HADMG control under dynamic and uncertain conditions.

The remainder of this article is structured according to the following framework. Chapter 2 provides a description of the operating principle and system configuration. Chapter 3 formulates the dynamical model for every single HADMG element. Chapter 4 outlines the design of the proposed controller. Lastly, Chapter 5 concludes by outlining the simulating results and discussion. Lastly, chapter 6 is conclusion.

Chapter 2

Operating principles and configuration of HADMG

The system setup and working principles of the suggested HADMG are covered in this section.

2.1. System Configuration

The overall design for the suggested HADMG is illustrated in Figure 1. A wind turbine generator linked to a PMSG and interfaced with the DC bus using a rectifier and a DC–DC boost converter (DDBC) and the solar PV unit that makes up this system is connected to the DC bus through a DDBC. Additionally, a bidirectional DC–DC converter (BDDC) is used to link the energy storage system (ESS) to the DC bus. Depending on the MG's power equilibrium, the ESS may operate in either discharging or charging mode. Hydrogen ESSs are coupled with an electrolyser and a proton exchange membrane fuel cell (PEMFC). The DC bus is linked to variable DC loads, and the AC bus is linked to variable AC loads. The rated voltage of the DC bus is 640 V, whereas the AC bus is rated at 220 V. The shared DC bus is linked to the AC bus through a three-phase BVSC equipped with an LC filter at the output. This configuration facilitates power management between the AC and DC components while maintaining a steady voltage on the DC bus inside the MG. The next section goes into great detail about this dynamic model.

2.2. Principles of Operation

To ensure a secure and reliable power supply, the HADMG must be designed to function well in a variety of operating modes regardless of variations in solar irradiation, wind speed, and loads. There are two possible operating modes for the proposed MG: islanded and grid-connected. To ensure a constant DC bus voltage and power transfer between the DC and AC buses, the BVSC is used in grid-tied mode. When the total DC-side output power surpasses the DC load requirement, the BVSC transfers power to the AC part. In contrast, the BVSC transfers power from the AC part to the DC part when the total output of DC power is insufficient to meet the whole DC load demand. Because the grid keeps a power equilibrium in this mode, the ESS is less important. This study does not encompass the grid-tied mode. In contrast, the ESS plays a crucial role in the HADMG's power control and stabilization of the voltage of the DC bus when in islanded operation. When the battery unit is fully charged, the FC uses the hydrogen gas that is generated by the electrolyser utilizing the available dc power. A BDDC maintains the power balance and voltage of the DC bus in the islanded operation based on the MG's different working conditions. It is important to balance power under different supply and load scenarios; these conditions can be shown as follows:

$$P_{pv} + P_{wind} \pm P_{BESS} = P_{(AC-load)} + P_{(DC-load)} + P_{Loss} \quad (1)$$

The terms PV system power, wind generator power, AC and DC load power, power loss, and battery power are represented by p_{wind},p_{pv}, $p_{(DC-load)}$, p_{BESS}, and p_{loss}, respectively. However, each MG unit's output power must be controlled in order to achieve the aforementioned power balance. Consequently, a proper mathematical representation of the MG units is essential for evaluating control solutions and developing them, as explained in the following section.

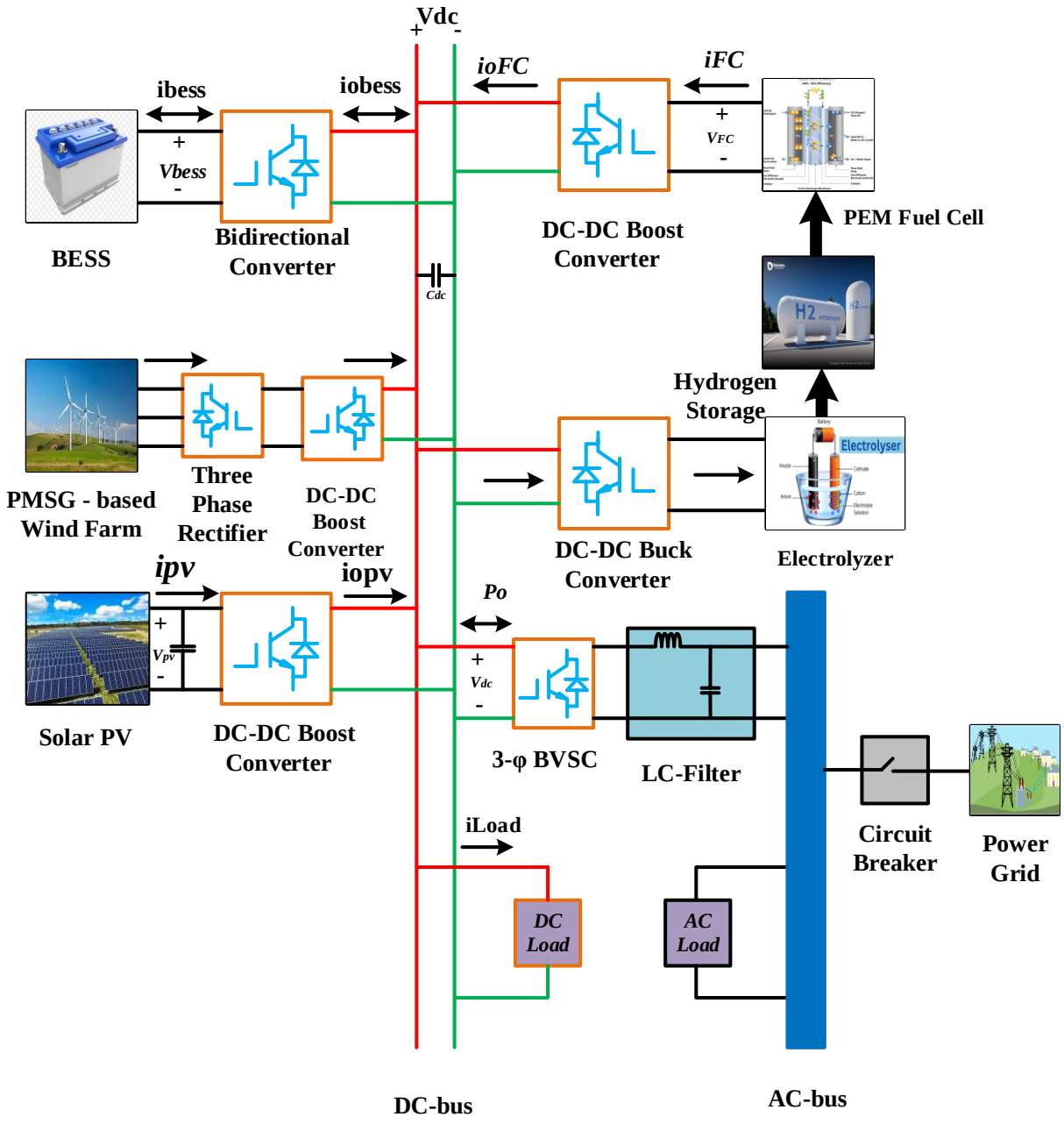


Figure 1: overall structure of the designed HADMG.

Chapter 3

Dynamical Model of Hybrid AC/DC Microgrid

The proposed controller will be developed utilizing the dynamic representations of every component in the suggested system. The proposed control approach is utilized to provide the control signal for A PMSG with a DDBC, a BESS with a BDDC, a PV unit with a DDBC, and a BVSC with an output LC filter. In the following sections, the dynamical representations of every of these components are explained.

3.1. Modeling of BVSC with an LC filter

Figure 2 shows an example of the BVSC's electrical circuits and LC filter. Figure 2 shows the electrical power converter dynamics which are required to design the controller suggested in this paper. Circuit theories, according to [40], are applied to derive these dynamics in the following ways:

$$\frac{dV_{dc}}{dt} = \frac{i_o}{C_{dc}} - \frac{3}{2V_{dc}C_{dc}} V_{cd} I_{od}$$

$$\frac{dV_{cd}}{dt} = \frac{1}{C_f} I_{id} + \omega V_{cq} - \frac{1}{C_f} I_{od}$$

$$\frac{dV_{cq}}{dt} = \frac{1}{C_f} I_{iq} - \omega V_{cd} - \frac{1}{C_f} I_{oq} \quad (2)$$

$$\frac{dI_{id}}{dt} = -\frac{1}{L_f} V_{cd} - \omega I_{iq} + \frac{1}{L_f} V_{dc} M_d$$

$$\frac{dI_{iq}}{dt} = -\frac{1}{L_f} V_{cq} - \omega I_{id} + \frac{1}{L_f} V_{dc} M_q$$

where the capacitor is denoted by $C_{dc}$and the DC-bus voltage by V_{dc}. A capacitor's voltage is shown on the d-axis by V_{cd} and on the q-axis by V_{cq}. Lf denotes the filter's inductor, whereas C_f stands for the filter's capacitor.

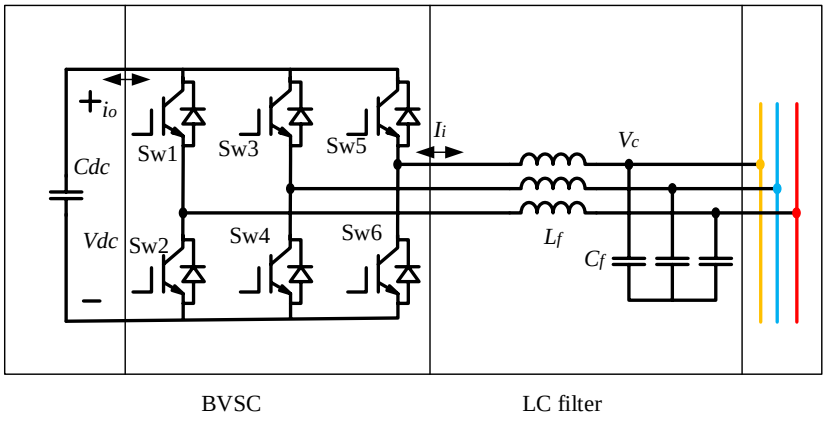


Figure 2: A BVSC equivalent circuit schematic with an output LC filter.

In a converter, the q-axis and d-axis denote the input current (I_{iq} andI_{id}, respectively), while the q-axis and d-axis denote the output current (I_{oq} and I_{od}, respectively). Lastly, ω represents the angular frequency. The model-based regulation method outlined in this section will be used to derive the control inputs, M_q andM_d.

3.2. Modeling of a solar PV unit with a DDBC

With the assumption that the photovoltaic cell is of the single diode configuration, the dynamics behavior of a DDBC-connected photovoltaic will be determined using the equivalent circuit shown in Figure 3. This dynamical representation can be expressed using the following equations [8]:

$$\frac{di_{Lpv}}{dt} = \frac{1}{L_{pv}}[-r_{pv}i_{Lpv} - (1-u_{pv})v_{dc} + v_{pv}]$$

$$\frac{dv_{dc}}{dt} = \frac{1}{C_{dc}}[(1-u_{pv})i_{Lpv} - i_{opv}] \quad (3)$$

The variables of the boost circuit are the input current i_{lpv}, the inductor L_{pv}, the internal resistance R_{pv}, the control input U_{pv}, and the output current i_{opv}.

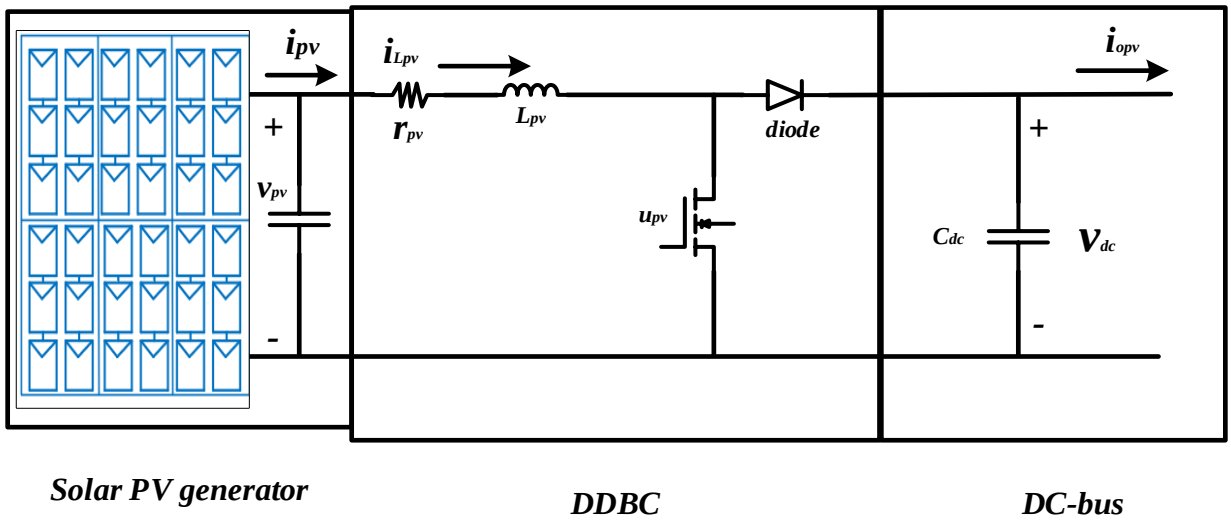


Figure 3: The solar PV's comparable circuit diagram with a DDBC.

Remark 1. This study uses the observe algorithm and perturb as a maximum power point tracking (MPPT) strategy to optimize the power output of the solar energy generation system.

3.3. Modeling of a PMSG unit with a DDBC

Figure 4 shows how the circuit of the rectifier is linked to the PMSG's stator and how a DDBC connects the circuit's output to the direct current bus. However, the controller for the PMSG generator is not designed to take into consideration the dynamics of the DC bus because they are already taken into account by the other components. The subsequent formula delineates the equations for the stator voltage of the PMSG within the rotor dq frame [16,17]:

$$v_{sd} = R_s i_{sd} + L_s(\frac{di_{sd}}{dt} - \omega_s i_{sq})$$

$$v_{sq} = R_s i_{sq} + L_s\left(\frac{di_{sq}}{dt} - \omega_s i_{sd}\right) + \omega_s \psi$$

(4)

where ψ for a machine's stator flux, ω_s stands for the angular frequency at synchronous speed, v_{sq} and $v_{sd}$for the voltage across the stator in the q and d-axis. In contrast, i_{sq} and$i_{sq}$for the current through the stator in the q and d-axis,R_s for the stator circuit's internal resistance, and L_s for the stator's inductance all represent variables of the PMSG generator. The stator of the PMSG generates the AC power, which a rectifier converter then transforms into DC electricity. The DC bus receives this power through the DDBC circuit.

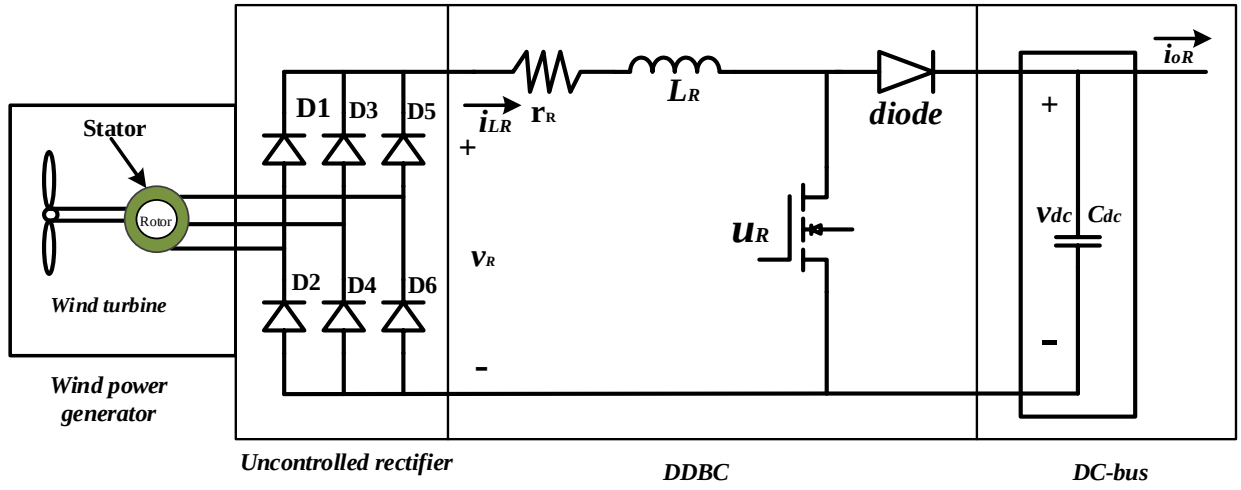


Figure 4: The equivalent circuit diagram for a wind power system with a DDBC.

The subsequent formula can be employed to ascertain the current in an unregulated rectifier circuit:

$$\frac{di_R}{dt} = \frac{1}{2L_s}(\frac{3\sqrt{6}}{\pi}E - v_R - \frac{3}{\pi}L_s\omega_s i_R) \quad (5)$$

where E, V_R, and i_R denote the current through the rectifier, the machine's output voltage, and the phase voltage of the rectifier circuit, respectively. The circuit's input current is supplied to the DC bus using a DDBC. The DDBC circuit's dynamic can, therefore, be described as follows:

$$\frac{di_{LR}}{dt} = \frac{1}{L_R}[-r_R i_{LR} - (1 - u_R)v_{dc} + v_R]$$

$$\frac{dv_{dc}}{dt} = \frac{1}{C_{dc}}[(1 - u_R)i_{LR} - i_{oR}] \quad (6)$$

The variables representing the rectifier circuit are as follows: $L_R$stands for its inductor, $i_{LR}$for the output current, $i_{OR}$for the boost circuit's output current, $r_R$for its internal resistance, and u_R for the boost circuit's control signal.

Remark 2: In this study, maximum PowerPoint tracking (MPPT) is accomplished by the best control of torque approach because of its simplicity and accuracy.

3.4. Modeling of a BESS unit with a BDDC

The power circuit of the BESS integrated with a BDDC is depicted in a simplified manner in Figure 5, from which a dynamic representation may be derived and articulated as [32]:

$$\frac{di_b}{dt} = \frac{1}{L_b}(v_b - r_b i_b - u_b v_{dc})$$

$$\frac{dv_{dc}}{dt} = \frac{1}{C_{dc}}(u_b i_b - i_{ob}) \quad (7)$$

where$i_{ob}$is the converter's output current, u_b is a BDDC's control input, r_b is its internal resistance, L_bL_b is its inductor, and v_b is the battery's terminal voltage. equation (7) describes the dynamical representation used to design the DBBC's switching control input. The next section provides the full controller design methodology, which formulates controllers using the dynamical systems of the different HADMG elements.

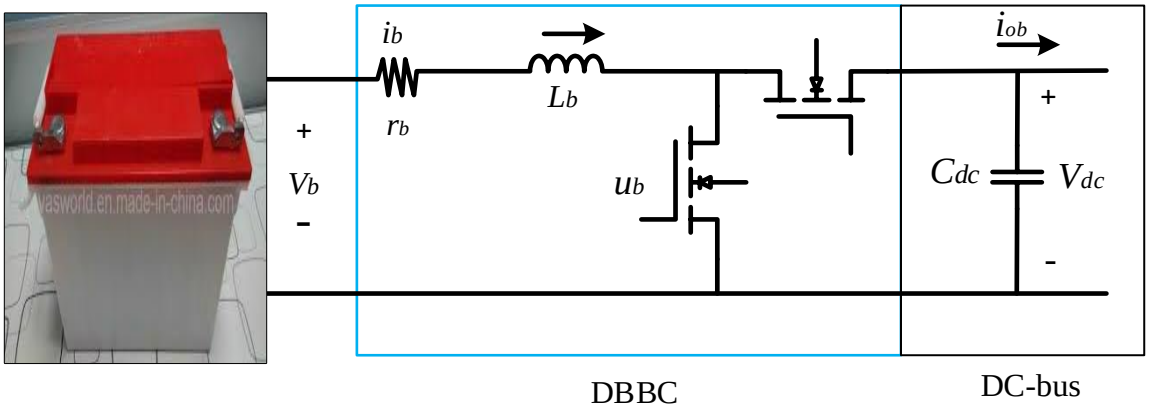


Figure 5: The simplified electrical circuit configuration of the BESS with a converter.

3.5. Modeling of a DDBC unit with a PEMFC

Because they can be used anywhere and at any weather, FCs are frequently used as a temporary energy source. Higher energy density, Higher efficiency, quick startup, quick response to changes, ease of maintenance, and slow degradation are the reasons why the hydrogen-powered PEMFC is preferred over existing FC models in this work [11]. The connection of a PEMFC to the DC microgrid typically involves a DDBC to step up the output voltage and maintain a stable DC bus. This converter regulates power flow from the fuel cell to the grid and ensures compatibility with other system components. The integration of such converters is crucial for maintaining voltage levels and controlling the dynamic behavior of the system under variable load and source conditions. For a DDBC connected to a PEMFC, the corresponding schematic illustration is shown in Figure 6.

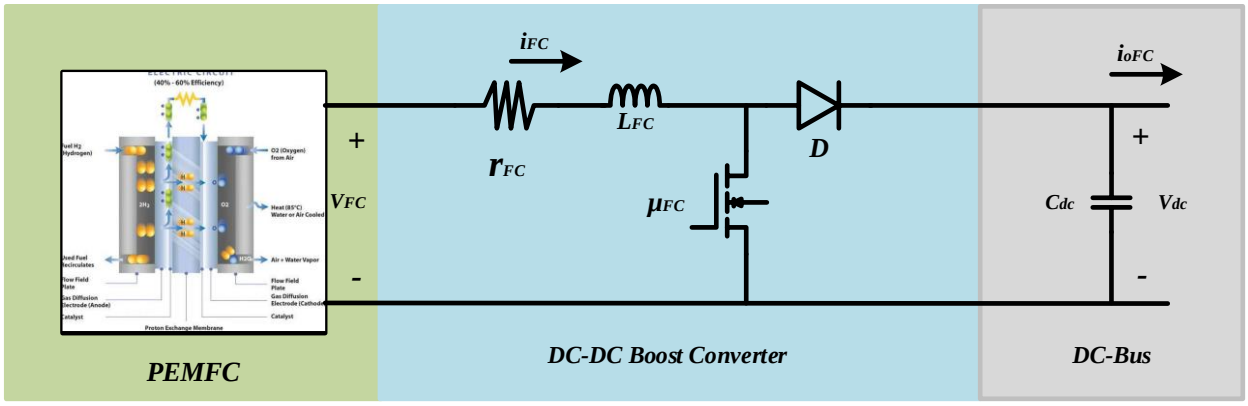


Figure 6: PEMFC-DDBC equivalent circuit.

The dynamical model is described by the subsequent formulas [11]:

$$\frac{dv_{dc}}{dt} = \frac{1}{C_{dc}}[(1-\mu_{FC})i_{FC} - i_{oFC}]$$

$$\frac{di_{FC}}{dt} = \frac{1}{L_{FC}}[v_{FC} - r_{FC}i_{FC} - (1-\mu_{FC})v_{dc}] \quad (8)$$

where i_{FC} is the current passing through the internal resistance (r_{FC}) and inductance (L_{FC}) of the DDBC, v_{FC} is the PEMFC's output voltage, $i_{oFC}$is the load current, and μ_{FC} is the control signal.

3.6. Modeling of an electrolyzer unit with a DC-DC buck converter

An electrolyzer unit equipped with a DC-DC buck converter is shown in Figure 7 with the corresponding schematic diagram.

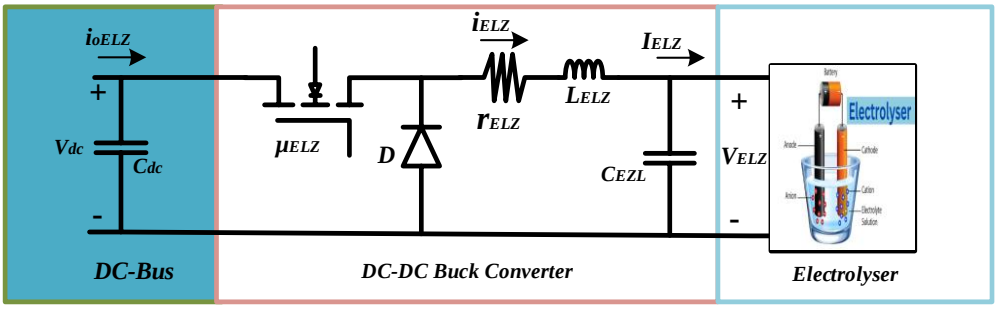


Figure 7: Equivalent circuit of an electrolyser with a DC-DC buck converter

The dynamical modeling is described by the next formulas [39]:

$$\frac{dv_{ELZ}}{dt} = \frac{1}{C_{ELZ}}[i_{ELZ} - I_{ELZ}]$$

$$\frac{di_{ELZ}}{dt} = \frac{1}{L_{ELZ}}[-v_{ELZ} - n_{ELZC}i_{ELZ} + \mu_{ELZ}v_{dc}] \quad (9)$$

where μ_{ELZ} is the control signal, v_{ELZ} is the electrolyzer's output voltage, i_{ELZ} is the output load current,i_{oELZ} is the input current, and i_{ELZ} is the current flowing through the DC-DC buck converter's resistance (r_{ELZ}) and inductance (L_{ELZ}).

Chapter 4

Design of the proposed controller

The suggested TSMBC produces the switching signals for control for every converter within this part. Since the proposed controller will be used for all elements of the suggested HADMG, the other elements get inputs for control from it. The detailed layout process of the suggested composite controller is explained in detail for the BVSC, which includes an LC filter.

The following section provides the full technique for designing a controller for the BVSC that includes an LC filter.

4.1. Modeling of a BVSC unit with a TSMBC

The voltage on the VSC side, in practice, increases or decreases in accordance with the power unbalance between generation and load. In the meantime, the modulation index of the controller on the VSC side decreases or increases to compensate for the power difference between load and generation. The modulation index exhibits greater oscillations as the power difference increases. In order to maintain the desired phase voltage and reduce fluctuations in voltage (i.e. E. 220 V (RMS)), a composite controller is introduced in this research, and the subsequent section goes into great detail about the process of design.

Step 1: If the intended magnitude of V_{dc} equals $V_{dc(ref)}$, the following formula can be used to define the tracking error:

$$e_{1VSC} = V_{dc} - V_{dc(ref)} \tag{10}$$

This error's dynamic is

$$\dot{e}_{1vsc} = \frac{i_o}{C_{dc}} - \frac{3}{2V_{dc}C_{dc}} V_{cd} I_{od} - V_{dc(ref)} \tag{11}$$

It is now necessary to analyze the steady-state behavior ofe_{1vsc}, which can be represented using the CLF as follows.

$$W_{1VSC} = \frac{1}{2} e_{1VSC}^2 \tag{12}$$

Remark 3: If w_{1vsc}, (e_{1vsc},) satisfies the next requirements, the equilibrium state is stable globally and asymptotically using Lyapunov's straightforward strategy:

- $W_{1vsc}(0) = 0$
- $W_{1vsc}(e_{1vsc}) > 0 \; for \; all \; e_{1vsc} \neq 0$
- $W_{1vsc}(e_{1vsc}) \rightarrow \infty \; 0 \; when \; \| \; e_{1vsc} \| \rightarrow \infty$
- $\dot{w}_{1vsc}(e_{1vsc}) < 0 \; for \; all \; e_{1vsc} \neq 0$

It is evident from equation (12) that the chosen Control Lyapunov Function satisfies the initial 3 requirements. The following is a possible representation of $\dot{w}_{1vsc}$ applying equation (11):

$$\dot{w}_{1vsc} = e_{1VSC}[\frac{i_o}{C_{dc}} - \frac{3}{2V_{dc}C_{dc}} V_{cd} I_{od} - \dot{V}_{dc(ref)}] \tag{13}$$

The stability function (α) that relates with respect to the V_{cd}, which is the state variable in equation (13), must be carefully chosen at this point in order to guarantee that e_{1vsc} converges to zero and accomplish V_{dc}= $V_{dc(ref)}$. To accomplish this, think about the options listed below:

$$V_{cd} = \alpha = \frac{2V_{dc}C_{dc}}{3I_{od}}\left(\frac{i_o}{C_{dc}} - \dot{V}_{dc(ref)} + K_{1VSC}e_{1VSC}\right) \quad (14)$$

Where the design variable k1VSC is optimistic, equation (13) can be changed as follows by using equation (14):

$$\dot{w}_{1vsc} = -k_{1VSC}e_{1VSC}^2 \quad (15)$$

Step 2: At this stage, the fault could be described as follows:

$$e_{2VSC} = V_{cd} - \alpha \quad (16)$$

Equation (2) can be used to express the e_{2VSC} dynamic as follows:

$$\dot{e}_{2vsc} = \frac{1}{C_f}I_{id} + \omega V_{cq} - \frac{1}{C_f}I_{od} - \dot{\alpha} \quad (17)$$

The following is a definition of the error in tracking (e_{3VSC}) that correlates to the target: the value of V_{cq}, represented as$V_{cq(ref)}$:

$$e_{3VSC} = V_{cq} - V_{cq(ref)} \quad (18)$$

As well as its derivative:

$$\dot{e}_{3VSC} = \frac{1}{C_f}I_{iq} - \omega V_{cd} - \frac{1}{C_f}I_{oq} - \dot{V}_{cq(ref)} \quad (19)$$

It is now possible to specify the Terminal Sliding Surface (TSS) of the d-axis as follows:

$$S_{d2} = e_{2VSC} + \beta_{d2}e_{2VSC}^{\frac{q}{p}} \quad (20)$$

Where the following requirement is fulfilled by the positive integers q and p, and βd2 > 0

p < 2q

Equation (17) can be used to express the dynamic ofS_{d2} in the following way:

$$\dot{S}_{d2} = \frac{1}{C_f}\tau_{d2}I_{id} + \tau_{d2}\omega V_{cq} - \frac{1}{C_f}\tau_{d2}I_{od} - \tau_{d2}\dot{\alpha} \quad (21)$$

Where $\tau_{d2} = 1 + \frac{q}{p}\beta_{d2}e_{2VSC}^{(\frac{q}{p}-1)}$ Thus, the dynamic of the q-axis TSS can be written in the following way:

$$\dot{S}_{q2} = \frac{1}{C_f}\tau_{q2}I_{iq} - \tau_{q2}\omega V_{cd} - \frac{1}{C_f}\tau_{q2}I_{oq} - \tau_{q2}\dot{V}_{cq(ref)} \quad (22)$$

Where $\tau_{q2} = 1 + \frac{q}{p}\beta_{q2}e_{3VSC}^{(\frac{q}{p}-1)}$ The subsequent method can now be used to select the CLF for this step:

$$W_{2VSC} = W_{1VSC} + \frac{1}{2}S_{d2}^2 + \frac{1}{2}S_{q2}^2 \quad (23)$$

The derivative ofW_{2VSC} can be written in the following manner:

$$\dot{W}_{2VSC} = -k_{1VSC}e_{1VSC}^2 + S_{d2}[\frac{1}{C_f}\tau_{d2}I_{id} + \tau_{d2}\omega V_{cq} - \frac{1}{C_f}\tau_{d2}I_{od} - \tau_{d2}\dot{\alpha}] + S_{q2}[\frac{1}{C_f}\tau_{q2}I_{iq} - \tau_{q2}\omega V_{cd} - \frac{1}{C_f}\tau_{q2}I_{oq} - \tau_{q2}\dot{V}_{cq(ref)}] \quad (24)$$

In order to ensure that $\dot{W}_{2VSC}$ is non-positive semi-definite at this point, i.e., When $\dot{W}_{2VSC} \leq 0$, the design can be filled using the reaching principle. Consequently,

$$\frac{1}{C_f}\tau_{d2}I_{id} + \tau_{d2}\omega V_{cq} - \frac{1}{C_f}\tau_{d2}I_{od} - \tau_{d2}\dot{\alpha} = -k_{d2}sgn(S_{d2})$$

$$\frac{1}{C_f}\tau_{q2}I_{iq} - \tau_{q2}\omega V_{cd} - \frac{1}{C_f}\tau_{q2}I_{oq} - \tau_{q2}\dot{V}_{cq(ref)} = -k_{q2}sgn(S_{q2}) \quad (25)$$

Using the positive control variables $k_{q2}$and k_{d2}. One obtains by substituting equation (25) into equation (24)

$$\dot{W}_{2VSC} = -k_{1VSC}e_{1VSC}^2 - k_{d2}|S_{d2}|^2 - k_{q2}\left|S_{q2}\right|^2 \quad (26)$$

with $S_{d2}sgn(S_{d2}) = |S_{d2}|$ and $S_{q2}sgn(S_{q2}) = |S_{q2}|$ accordingly. The optimal approach for determining the virtual control theory of the controller is as follows:

$$I_{id} = \alpha_d = \frac{C_f}{(\tau_{d2}I_{id})}[\frac{1}{C_f}\tau_{d2}I_{od} + \tau_{d2}\dot{\alpha} - \tau_{d2}\omega V_{cq} - k_{d2}sgn(S_{d2})]$$

$$I_{iq} = \alpha_q = \frac{C_f}{\tau_{q2}I_{iq}}[\frac{1}{C_f}\tau_{q2}I_{oq} + \tau_{q2}\dot{V}_{cq(ref)} + \tau_{q2}\omega V_{cd} - k_{q2}sgn(S_{q2})] \quad (27)$$

Step 3: involves defining αq and αd in relation to their mistake parameters. This is due to being connected with states $I_{id}$and I_{iq}, correspondingly:

$$e_{4VSC} = I_{id} - \alpha_d$$

$$e_{5VSC} = I_{iq} - \alpha_q \quad (28)$$

The subsequent formulas delineate the dynamics associated with these mistake parameters:

$$\dot{e}_{4VSC} = -\frac{1}{L_f}V_{cd} - \omega I_{iq} + \frac{1}{L_f}V_{dc}M_d - \dot{\alpha}_d$$

$$\dot{e}_{5VSC} = -\frac{1}{L_f}V_{cq} - \omega I_{id} + \frac{1}{L_f}V_{dc}M_q - \dot{\alpha}_q \quad (29)$$

The TSS can currently be described in the following manner:

$$S_{d3} = e_{4VSC} + \beta_{d3}e_{4VSC}^{\frac{q}{p}}$$

$$S_{q3} = e_{5VSC} + \beta_{q3}e_{5VSC}^{\frac{q}{p}} \quad (30)$$

Through the use of equation (29), the behavior of equation (30) is available in the following manner:

$$\dot{S}_{d3} = (-\frac{1}{L_f}V_{cd} + \omega I_{iq} + \frac{1}{L_f}V_{dc}M_d - \dot{\alpha}_d)(1 + \beta_{d3}\frac{q}{p}e_{4VSC}^{\left(\frac{q}{p}-1\right)})$$

$$\dot{S}_{q3} = (-\frac{1}{L_f}V_{cq} - \omega I_{id} + \frac{1}{L_f}V_{dc}M_q - \dot{\alpha}_q)(1 + \beta_{q3}\frac{q}{p}e_{5VSC}^{\left(\frac{q}{p}-1\right)}) \quad (31)$$

The ultimate CLF must be determined in the manner described below in order to examine the meeting of all BVSC-related faults.

$$W_{3VSC} = W_{2VSC} + \frac{1}{2}S_{d3}^2 + \frac{1}{2}S_{q3}^2 \quad (32)$$

Whose derivative is expressed as follows:

$$\dot{W}_{3VSC} = -k_{1VSC}e_{1VSC}^2 - k_{d2}|S_{d2}|^2 - k_{q2}|S_{q2}|^2 + S_{d3}[(-\frac{1}{L_f}V_{cd} + \omega I_{iq} + \frac{1}{L_f}V_{dc}M_d - \dot{\alpha}_d)(1 +$$
$$\beta_{d3}\frac{q}{p}e_{4VSC}^{\left(\frac{q}{p}-1\right)})] + S_{q3}[(-\frac{1}{L_f}V_{cq} - \omega I_{id} + \frac{1}{L_f}V_{dc}M_q - \dot{\alpha}_q)(1 + \beta_{q3}\frac{q}{p}e_{5VSC}^{\left(\frac{q}{p}-1\right)})] \quad (33)$$

To guarantee the stability of the converter as a whole, $\dot{W}_{3VSC}$in equation (33) ought to be either negative-definite or negative semi-definite, i.e. e. $\dot{W}_{3VSC} \leq 0$. This could be accomplished by carefully choosing M_d and M_q in the manner described below.

$$M_d = \frac{L_f}{V_{dc}(1 + \beta_{d3}\frac{q}{p}e_{4VSC}^{\left(\frac{q}{p}-1\right)})}[(-\frac{1}{L_f}V_{cd} + \omega I_{iq} + \frac{1}{L_f}V_{dc}M_q - \dot{\alpha}_d) \times (1 + \beta_{d3}\frac{q}{p}e_{4VSC}^{\left(\frac{q}{p}-1\right)}) - k_{d3}sgn(S_{d3})]$$

$$M_q = \frac{L_f}{V_{dc}(1+\beta_{q3}\frac{q}{p}e_{5VSC}^{\left(\frac{q}{p}-1\right)})}[(-\frac{1}{L_f}V_{cq} - \omega I_{id} + \frac{1}{L_f}V_{dc}M_q - \dot{\alpha}_q) \times (1 + \beta_{q3}\frac{q}{p}e_{5VSC}^{\left(\frac{q}{p}-1\right)}) - k_{q3}sgn(S_{q3})] \quad (34)$$

Where the positive variables for control are kq3 and kd3. Applying equation (34), equation (33) what produces is as follows.

$$\dot{W}_{3VSC} = -k_{1VSC}e_{1VSC}^2 - k_{d2}|S_{d2}|^2 - k_{q2}|S_{q^2}|^2 - k_{d3}|S_{d3}|^2 - k_{q3}|S_{q^3}|^2 \quad (35)$$

Remark 4. The subsequent criteria is fulfilled as the mistake will reach the TSS within a certain timeframe:

$$t_r = \frac{S(0)}{\eta} \quad (36)$$

where S(0) is S(t)'s starting value. Once more, the calculation for another certain timeframe (t_s) is as follows:

$$\dot{e} = -\frac{q}{p}\beta e^{\frac{q}{p}-1} \quad (37)$$

It can be rewritten in the following manner:

$$dt = -\frac{p}{\beta q}e^{1-\frac{q}{p}}de \quad (38)$$

Combining both sides of the equation. (38) provides the following results for determining t_s that moves from e(tr)/= 0 to e$(t_r + t_s)$ = 0:$e(t_r) \neq 0\ to\ e(t_r + t_s) = 0, yields$

$$t_s = \frac{p}{\beta q(2-\frac{q}{p})}[e(t_r)^{2-\frac{q}{p}} - 1 \quad (39)$$

The tracking fault as well as its derivative can therefore be ensured to converge in a limited amount of time by the suggested control approach:

Remark 5. Each of the user-defined fixed values are presumed to meet the next requirement:

$$k_{1VSC} > 0,\ k_{d2} > 0,\ k_{d3} > 0,\ k_{q2} > 0, and\ \ k_{q3} > 0 \quad (40)$$

Applying the requirements for inequality outlined in (40), equation (35) can be reformulated as follows:

$$\dot{W}_{3VSC} \leq -k_{1VSC}e_{1VSC}^2 - k_{d2}|S_{d2}|^2 - k_{q2}|S_{q2}|^2 - k_{d3}|S_{d3}|^2 - k_{q3}|S_{q3}|^2 \leq 0 \quad (41)$$

when the two sides of equation (41) are combined, the outcome is:

$$\int_0^\infty dW_{3VSC} \leq -k_{1VSC}\int_0^\infty e_{1VSC}^2 dt - k_{d2}\int_0^\infty |S_{d2}|^2 d2 - k_{q2}\int_0^\infty |S_{q2}|^2 dt - k_{d3}\int_0^\infty |S_{d3}|^2\, dt - k_{q3}\int_0^\infty |S_{q3}|^2\, dt$$
(42)

Or

$$W_{3VSC}(\infty) - W_{3VSC}(0) \leq -k_{1VSC}\int_0^\infty e_{1VSC}^2 dt - k_{d2}\int_0^\infty |S_{d2}|^2\, dt - k_{q2}\int_0^\infty |S_{q2}|^2\, dt - k_{d3}\int_0^\infty |S_{d3}|^2 dt - k_{q3}\int_0^\infty |S_{q3}|^2 dt \quad (43)$$

equation (43) can be reformulated as

$$k_{1VSC}\int_0^\infty e_{1VSC}^2\, dt + k_{d2}\int_0^\infty |S_{d2}|^2\, dt + k_{q2}\int_0^\infty |S_{q2}|^2\, dt + k_{d3}\int_0^\infty |S_{d3}|^2 dt + k_{q3}\int_0^\infty |S_{q3}|^2 dt \leq W_{3VSC}(0) - W_{3VSC}(\infty) \quad (44)$$

Since $W_{3VSC}(\infty) \geq 0$, and

$$\int_0^\infty e_{1VSC}^2\, dt < \infty, \int_0^\infty |S_{d2}|^2 dt\ < \infty, \int_0^\infty |S_{d3}|^2 dt < \infty, \int_0^\infty |S_{q2}|^2 dt < \infty, and\ \int_0^\infty |S_{q3}|^2 dt < \infty\ holds\ k_{1VSC}\int_0^\infty e_{1VSC}^2\, dt + k_{d2}\int_0^\infty |S_{d2}|^2 dt + k_{q2}\int_0^\infty |S_{q2}|^2\, dt + k_{d3}\int_0^\infty |S_{d3}|^2 dt + k_{q3}\int_0^\infty |S_{q3}|^2 dt \leq W_{3VSC}(0) = 0 \quad (45)$$

The fact that $e_{ivsc} \rightarrow 0$ with i = 1, 2, 3, 4, 5, $s_{d2} \rightarrow 0$, and $s_{d3} \rightarrow 0$, $s_{d2} \rightarrow 0$, Sd3 $\rightarrow 0$ as t $\rightarrow \infty$ is evident from equations (43) and (45). Therefore, the suggested controller satisfies the reliability requirements for the entire BVSC network with an LC filter at the output.

Remark 6. Using comparable techniques, one can ascertain the control inputs for additional converters. For the sake of conciseness, this study does not go into great detail about the specific design techniques for these converters.

4.2. Design of the PV's TSMBC in combination with a DDBC

Equation (3) describes the time-dependent model that is used to obtain the control input from DDBC with the PV network. Now, the DDBC's control input statement is delineated below, employing the TSMBC approach.

$$\dot{u}_{pv} = -\frac{1}{V_{dc}(1+\beta_{pv}\frac{q}{p}e_{2pv}^{(\frac{q}{p}-1)})}\left[M_1 + M_2 + K_{2pv}sgn(S_{pv})\right] \tag{46}$$

Where e_{1pv} and e_{2pv} are error variables; and $M_1 = \frac{1}{L_{pv}}[-r_{pv}\dot{i}_{Lpv} - (1-u_{pv})\dot{v}_{pv}], M_2 = K_{1pv}\dot{e}_{1pv} - \dddot{\iota}_{Lpv}$ with K_{1pv} and K_{2pv} as positive control parameters.

Remark 7. Since it is comparable to the BVSC network, the Lyapunov stability demonstration of the solar PV unit utilizing a DDBC control structure is left out.

4.3. TSMBC design for the BDDC in conjunction with a rectifier for a PMSG

For a PMSG, the control data input for the DDBC within the rectifying device is shown by equation (6), shall be obtained by means of the TSMBC methodology. This is how the control input statement is produced.

$$\dot{u}_R = -\frac{L_R}{V_{dc}(1+\beta_R\frac{q}{p}e_{2R}^{(\frac{q}{p}-1)})}\left[\dot{A}_R + u_R\dot{V}_{dc} + K_{2R}sgn(S_R)\right] \tag{47}$$

where $A_r = \frac{1}{L_R}[-r_R i_{LR} - (1-u_R)V_{dc} + V_R] - \ddot{i}_{LR} + K_{1R}e_{1R}$ and e_{1R} and e_{2R} arefault parameter with K_{1R} and K_{2R}as a positive control variable.

Remark 8. Because it is comparable to the BVSC network, the Lyapunov stability demonstration of the PMSG with a DDBC control network is also left out.

4.4. TSMBC design for the BDDC in conjunction with the BESS

Equation (10) is used to determine the switching signal of control for the BDDC within a BESS. The TSMBC method is now used to derive the control input statement as below

$$\dot{u}_b = -\frac{L_b}{V_{dc}(1+\beta_b \frac{q}{p} e_{2b}^{(\frac{q}{p}-1)})}[M_b + K_{2b} sgn(S_b)] \tag{48}$$

where e_{1b} and e_{2b} are error variables; and

$M_b = \frac{1}{L_b}(\dot{v}_b - \dot{r}_b \dot{i}_b - u_b v_{dc}) - \dot{i}_{b(ref)} + K_{1b}\dot{e}_b$ with K_{1b} and K_{2b} as positive control parameters.

Remark 9. Since the BESS with a BDDC control network is comparable to the BVSC network, the Lyapunov stability demonstration is left out.

With the help of the generated control inputs for different elements, the HADMG's performance is investigated. The following section looks at these designed controllers' effectiveness in a variety of operating conditions.

Chapter 5

Simulation Results and Discussion

This section illustrates how the suggested controller improves a HADMG's power management while providing accurate tracking and transient voltage stability on the DC bus despite major disruptions. To accomplish that, the Matlab / Simulink software is used to build a HADMG system, as shown in Figure 1. The following sections contain the control parameters, implementation block diagram, parameters, and several case studies for examining the HADMG system.

5.1. Selection of simulation parameters

Considering typical climatic conditions, the PV cell's highest possible rating of power is 10 kW and the intended voltage for the DC bus is 640 V. It is anticipated that the PMSG-based wind power plant will have a 25 kW rated production capacity. A theoretical voltage of 300 V and a lithium-ion battery with a 200 Ah capacity is utilized for the BESS. The highest possible load demand for an AC bus is 30 kW, while the highest possible load demand for a DC bus is 25 kW. Every converter frequency for switching is set to 5 kHz within the simulation, and 10 kHz is used as the frequency of sampling. Table 1 currently provides a summary of each of these. Furthermore, every user-defined characteristic of the suggested controller, as shown in Table 2, is selected through an experimentation procedure whereby the variable values are progressively changed until the intended outcome is achieved. To better learn about the suggested controller, the implementation block diagram is provided in the following subsection before the simulation outcomes are discussed.

Remark 10. Notably, to reduce the losses and complexity of distribution systems, suitable voltage limitations are introduced. Since standardization is difficult, publications have suggested a variety of voltage ratings for distribution networks, from 12 V to 800 V. Despite ongoing efforts to improve these benchmarks, these levels of DC voltage may be impacted by the typical application areas that are now in place, such as data centers that operate on 380–400 V, camping vehicles for road transport that use 12–24 V, and telecommunication applications that use 48 V. When using large electrical equipment, the safest way to prevent malfunctions and fire threats is to overestimate the power. This is because Watt Volt = Amp states that a 50% decrease in amperage occurs for every twice rise in voltage. By lowering the electric current within the DC network, a greater range of items, including fuses and wires, will be available for a certain arrangement. Therefore, 640 V DC bus voltage is taken into account in this work to achieve this goal. Additionally, this study takes into account a common AC bus voltage of 220 V (RMS).

Remark 11. This comment discusses how to choose controller gains. Notably, choosing the right parameters is crucial for any kind of control technique in order to produce fast convergence control and reliable control performance.

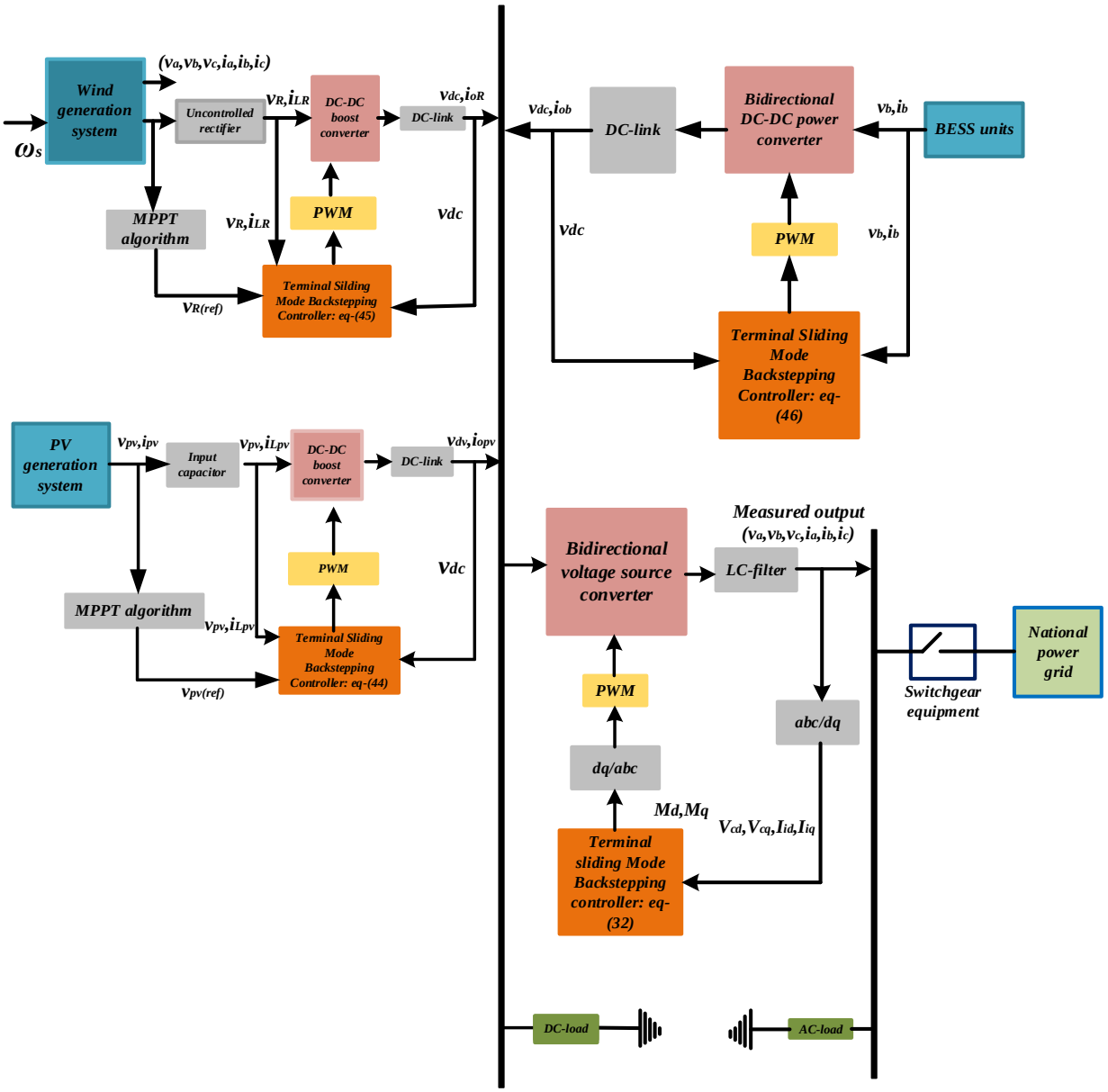


Figure 8: Implementation structure of the proposed HADMG with a nonlinear control scheme.

Designing and deploying new controllers has several goals, one of which is to improve behavior during the transient period. In the suggested method, significant values of these design variables may ensure quick transient performance. However, substantial amounts of these gains are not always beneficial since they give an undesirable disapproval of disturbances and increase overshoot, which degrades the controller's performance. Furthermore, controlling signal saturation may arise from over-increasing design variables. Thus, it is important to consider a suitable trade-off between the optimum gains and the other performance parameters, including settling time, percentage overshoot, etc. All of these variables are taken into consideration while the simulation is being run in this work to optimize the gain of user-defined parameters.

5.2. Block diagram of the implementation

The standardized deployment block design of the recommended control strategy is shown in Figure 8. Chapter 4 may indicate that a thorough calculation is required to determine the ultimate control signal. However, the planned controller simply utilizes current and voltage as mechanical system attributes to execute this control signal. These nominal values and physical characteristics of different elements are used to create the control signal, which is then fed to every MG element's switch via the appropriate pulse width modulator. The MATLAB / SIMULINK software provides the control signals for every HADMG element. As explained in the next part, the efficiency of the recommended control approach is evaluated for several kinds of HADMG scenarios, including variations in solar PV array irradiance, variations in wind speed, variations in both AC and DC load demand scenarios, and so forth. Additionally, the controller's adaptability allows it to respond dynamically to real-time fluctuations in system parameters, ensuring stable operation under varying conditions. Its ability to regulate voltage and power flow efficiently makes it suitable for complex MG applications, where renewable energy sources introduce high levels of intermittency. By maintaining precise control over transient responses, the proposed strategy significantly enhances the microgrid's reliability and resilience against external disturbances.

5.3. Simulation results

The DC bus voltage of the proposed hybrid MG is regulated by the operation of the photovoltaic generator unit. Subsequently, the wind generator will be initiated and integrated into operation, followed by the other components, including the BESS, DC load, and AC load. Diverse operating scenarios may occur inside the proposed system. To validate the efficacy of the created controller in regulating the DC and AC bus voltages while supplying power to loads, the subsequent two scenarios are selected:

- Controller performance when the electricity generated varies and
- Performance of the controller when the load demand varies

The effectiveness of the devised controller is contrasted with an existing double integral sliding mode controller (EDISMC), as suggested in [37], to demonstrate its superiority. These two scenarios were chosen because they reflect the most common and impactful operational disturbances in microgrids. By evaluating the controller's performance under generation variability and load fluctuations, the system's robustness, adaptability, and control accuracy can be effectively assessed. This ensures a realistic validation of the proposed control strategy in maintaining stable operation under dynamic conditions. To implement and simulate the proposed control strategy, accurate modeling of all system components was required. The electrical parameters of the simulated hybrid AC/DC MG, including the PV unit, wind generator, BESS, and common DC bus, are summarized in Table 1.

Table 1: Parameters of the simulated hybrid AC/DC microgrid

Solar photovoltaic unit	
Parameters	Values
Maximum output power, P_{pv}	10 kW
Internal resistance of the DDBC, r_{pv}	50 mΩ
Inductance of the DDBC,L_{pv}	0.352 mH
Permanent magnet SG unit	
Maximum output power,P_{wind}	25 kW
Resistance of a stator,R_s	425 mΩ
Inductance of a stator,L_s	1.67 mH
Stator flux, ψ	0.433
Resistance of the DDBC,r_R	40 mΩ
Inductance of the DDBC, L_R	0.2 mH
Lithium-ion battery energy storage system	
Nominal voltage, v_b	300 V
Rated capacity, Q_b	200 Ah
Resistance of the converter, r_b	80 mΩ
Inductance of the converter, L_b	1 mH
Common DC bus	
Nominal voltage of a DC bus, $V_{(dc-ref)}$	640 V
Capacitance of a DC bus, C_{dc}	1200 µF
DC load	0~25 kW
Bidirectional voltage source converter	
Filter capacitor, C_f	6.85 µF
Filter inductor, L_f	2 mH
AC load	0~30 kW

Table 2: Control parameters

Control parameters for a BVSC	
Parameters	Values
k_{1VSC}, k_{d2}, k_{q2}, k_{d3}, k_{q3} β_{d2}, β_{q2}, β_{d3}, β_{q3}, p, q	250, 300, 150, 450, 650 80, 110, 70, 85, 5, 3
Control parameters for a solar PV unit	
K_{1pv}, K_{2pv}, β_{pv}, p, q	270, 310, 150, 5, 3
Control parameters for a PMSG unit	
K_{1R}, K_{2R}, β_R, p, q	450, 600, 80, 5, 3
Control parameters for a BESS unit	
K_{1b}, K_{2b}, β_b, p, q	350, 380, 90, 5, 3

Table 3: Power flows of Figure 9

Power flows	After transient t = 1.5 s	After transient t = 4 s	After transient t = 6 s	After transient t = 7 s
P_{PV} (KW)	7.467	5.413	5.413	9.522
P_{wind} (KW)	18.47	18.47	13.75	13.75
$P_{DC-load}$ (KW)	5.852	5.852	5.852	5.852
$P_{AC-load}$ (KW)	15.43	15.43	15.43	15.43
P_{BESS} (KW)	-1.24	0.8	5.03	0.93

- **Case I:** Controller performance under variation of the Renewable Energy

The performance of the suggested controller is evaluated in this case study by taking into account variations in solar irradiance in the solar PV unit and varied wind speeds for the PMSG. Additionally, it is assumed that the AC demand and DC load are both fixed at 15.43 kW and 5.852 kW, respectively. Furthermore, since the PV unit's irradiance value is set at 900 W/m2, or 8.493 kW of output power, it is assumed that it does not initially operate under typical weather circumstances. This process is repeated until t = 1.5 s.

However, prior to t = 6 s, the wind speed was 12 m/s, and the PMSG-based wind farm generates 13.70 kW of power at this wind speed. Consequently, the DC-side total power during the 0–1.5 s interval is 26.963 kW, whereas the total load demand is 5.852 kW, meaning that an extra 21.111 kW is available. Depending on the load's need and the BESS's SoC level, this additional power can either be transferred to the AC side or stored in the battery. However, the AC load requirement is 15.43 kW, and the grid or the DC side's power will be used to meet this load demand. However, because it operates in an islanded mode and this study does not take grid connection into account, 15.430 kW of AC load power must be imported from the DC side. This may be easily done by modulating the BVSC's control input. Since it stays below the battery's maximum charging limit, the remaining power, or 5.681 kW, will be stored in the battery. Nevertheless, the battery will charge the remaining 2.320 kW of power after the system loss reaches 3.610 kW. As seen in Figure 9, all of this is now apparent in the power profiles of individual components until t = 1.5 s. In Figure 10, the matching DC bus is displayed. However, because transients are absent from the MG until t = 1.5 s, it is challenging to discern from these responses the differences between the proposed controller and the current controller. Variations in performance during temporary contexts, however, can be identified in the section that follows. As shown in Figure 9(a), the output power decreases from 8.493 kW to 7.467 kW at t = 1.5 s due to a decrease in solar irradiation from 900 W/m^2 to 800 W/m^2.

Table 4: Quantitative analysis of a PV unit

Transient time (s)	Settling time (ms)			Overshoot (%)		
	TSMBC	EDISMC	Performance Improved (%)	TSMBC	EDISMC	Performance Improved (%)
1.5	2.5	250	99	0	2.90	100
4	2.5	250	99	0	7.96	100
7	2.5	250	99	0	9.22	100

This process is continued until t = 3 s, while all other conditions remain unchanged. The overall generation still exceeds the total load demand, as seen in Figures. 9(a) and (b). Consequently, the DC side's generated power can be exported to the AC side or retained in the BESS as previously indicated in order to maintain power balance. As illustrated in Figure9(e), the BESS will now retain less power because the net power surplus after exporting to the AC side is less than in the preceding stage. Figures9 and 10 show the transient behaviour of the DC bus voltage and the power waveforms for every unit at t = 1.5s. Nonetheless, the suggested controller manages transients better than the current controller.

At t = 4s, the HADMG undergoes another transient as the output power of the PV unit drops from 7.46 kW to 5.413 kW due to a fall in solar irradiation from 800 W/m^2 to 600 W/m^2. The power profiles of the remaining loads and generating units are then compared to the operating scenario from t = 4s to t = 6s. The BESS shifts to discharge in order to maintain the system power balance during this period as total power is less than the demand for the entire load. Figures 9 and 10 show the related power profile and DC bus responses, respectively.

The wind speed drops from 12 m/s to 9 m/s, causing a rapid drop in wind generator output from 18.47 kW to 13.75 kW. This will continue until t = 10 s, disrupting the HADMG's power profiles. And this process keeps going until t = 7s, with all other conditions staying the same. In this instance, the BVSC will export energy from the DC side to the AC side. However, as seen in Figure9(e), there is still insufficient power to meet the load requirement, which will be made up for by the BESS. This functional scenario continues until

t = 6s. This transient is slightly more severe than the previous one, as can be seen by looking at the voltage at the DC bus in Figure 10.

Again, when the solar irradiation rises from 600 W/m2 to 950 W/m^2, the PV panel output is approximately 9.522 kW at t = 7s. At this point, the BESS is still releasing power to maintain the power balance because the amount of electric power generated is greater than it was in the prior time period but less than the overall demand. The matching power profiles and DC bus voltage for the suggested controller and the current controller are shown in Figures9 and 10. It is evident that the suggested controller responds to the power profile and DC bus voltage more smoothly than the current controllers. To help with comprehension, Table 3 also provides a comprehensive summary of the power flow shown in Figure9. The performance of the developed controller is contrasted with that of the current controller in terms of percentage overshoot and settling time under different operating scenarios, as previously mentioned in this case study. As shown in Tables 4–9, the planned controller output outperforms the current controller in terms of overshoot and settling time, as shown in Figures 9 and 10.

- **Case 2:** Controller performance under variation of the load demand

It is commonly known that variations in load demand are common in all power systems, particularly when MG functioning is taken into account.

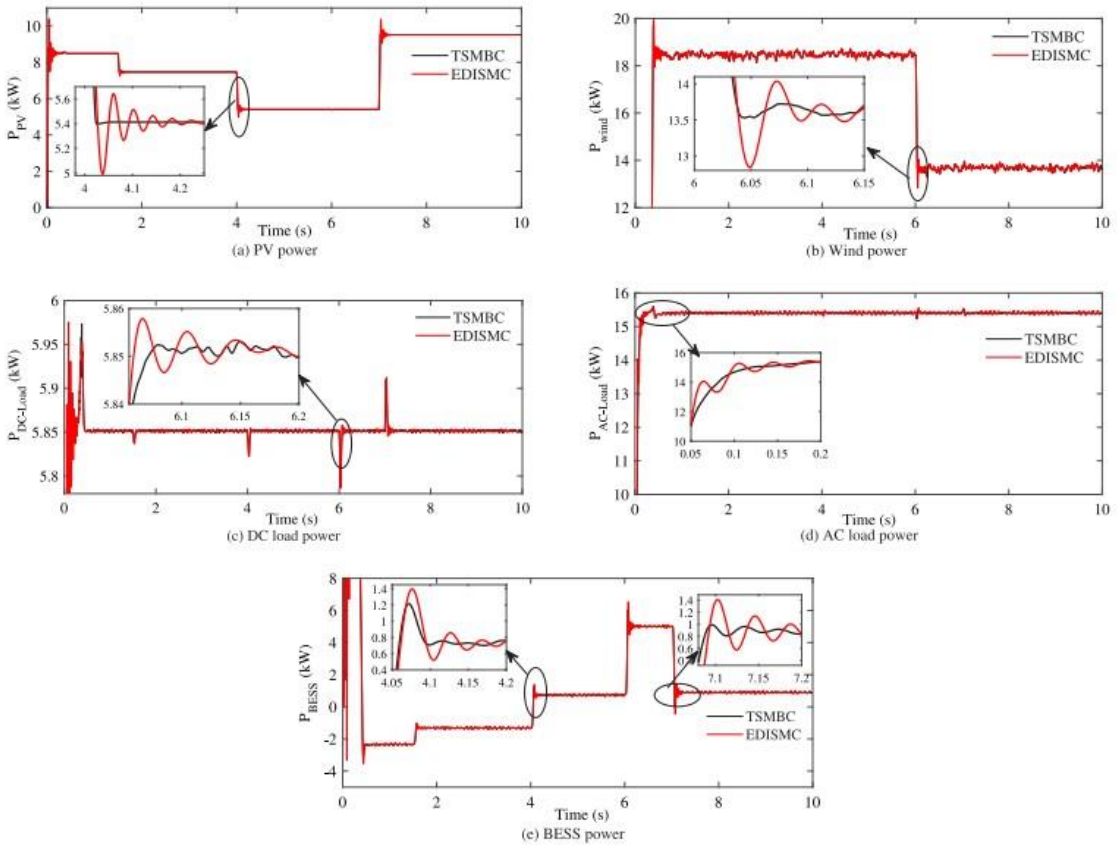


Figure 9: Dynamic stability of the solar PV system, wind generator system, DC load power, AC load power, and BESS power under case I

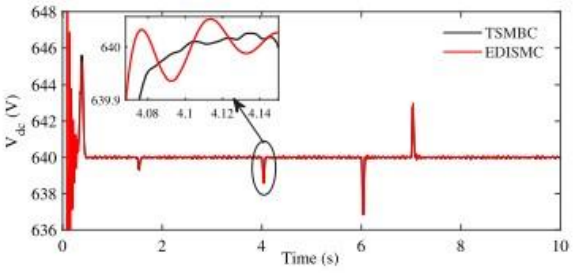


Figure 10: Dynamic stability of the DC bus under case I

Table 5: Quantitative analysis for a PMSG unit

Transient time (s)	Settling time (ms)			Overshoot (%)		
	TSMBC	EDISMC	Performance Improved (%)	TSMBC	EDISMC	Performance Improved (%)
6	100	200	50	0	6.90	100

Table 6: Quantitative analysis for a DC load power

Transient time (s)	Settling time (ms)			Overshoot (%)		
	TSMBC	EDISMC	Performance Improved (%)	TSMBC	EDISMC	Performance Improved (%)
1.5	60	110	45.45	0.20	0.88	77.27
3	20	200	90	0	11.25	100
4	82	210	60.95	0	0.5	100
6	20	200	90	0	31.64	100
7	68	192	64.58	0	0.21	100

Table 7: Quantitative analysis for a AC load power

Transient time (s)	Settling time (ms)			Overshoot (%)		
	TSMBC	EDISMC	Performance Improved (%)	TSMBC	EDISMC	Performance Improved (%)
5	60	200	70	0	5.40	100
8	2.550	200	98.73	0	16.76	100

Table 8: Quantitative analysis for a BESS unit

Transient time (s)	Settling time (ms)			Overshoot (%)		
	TSMBC	EDISMC	Performance Improved (%)	TSMBC	EDISMC	Performance Improved (%)
1.5	80	150	46.66	7.69	23.07	66.66
3	110	220	50	46.34	82.92	44.115
4	100	200	50	50	75	33.33
5	110	220	50	13.74	20.56	33.17
6	130	250	48	20	57.50	65.22
7	110	250	56	11.11	55.55	80
8	130	260	50	13.33	35	61.91

In light of this, the variations in the DC and AC load demand powers are thought to demonstrate the efficacy of the suggested controller in this particular circumstance. As shown in Figures 11(a) and 11(b), respectively, it is also assumed in this case study that the PV unit and PMSG will generate 9.520 kW and 13.660 kW of power, respectively, until t = 10s. However, as shown in Figures 11(c) and 11(d), the DC load and AC load demand are adjusted to 5.852 kW and 8.410 kW, respectively, prior to the transient, i.e., t = 0 3s. During this time, the aggregate load demand is 14.262 kW, while the total generation is 23.160 kW. As a result, the battery will store the 8.890 kW of excess power. However, the battery's charging power is 6.030 kW, meaning that the system's power loss is 2.860 kW.

Table 9: Quantitative analysis for a DC bus voltage

Transient time (s)	Settling time (ms)			Overshoot (%)		
	TSMBC	EDISMC	Performance Improved (%)	TSMBC	EDISMC	Performance Improved (%)
1.5	60	90	33.33	0	0.00402	100
3	100	200	50	0	0.03125	100
4	100	150	33.33	0	0.0078	100
5	110	220	50	0	0.03125	100
6	100	220	54.54	0	0.03125	100
7	100	200	50	0	0.03125	100
8	100	210	52.38	0	0.03125	100

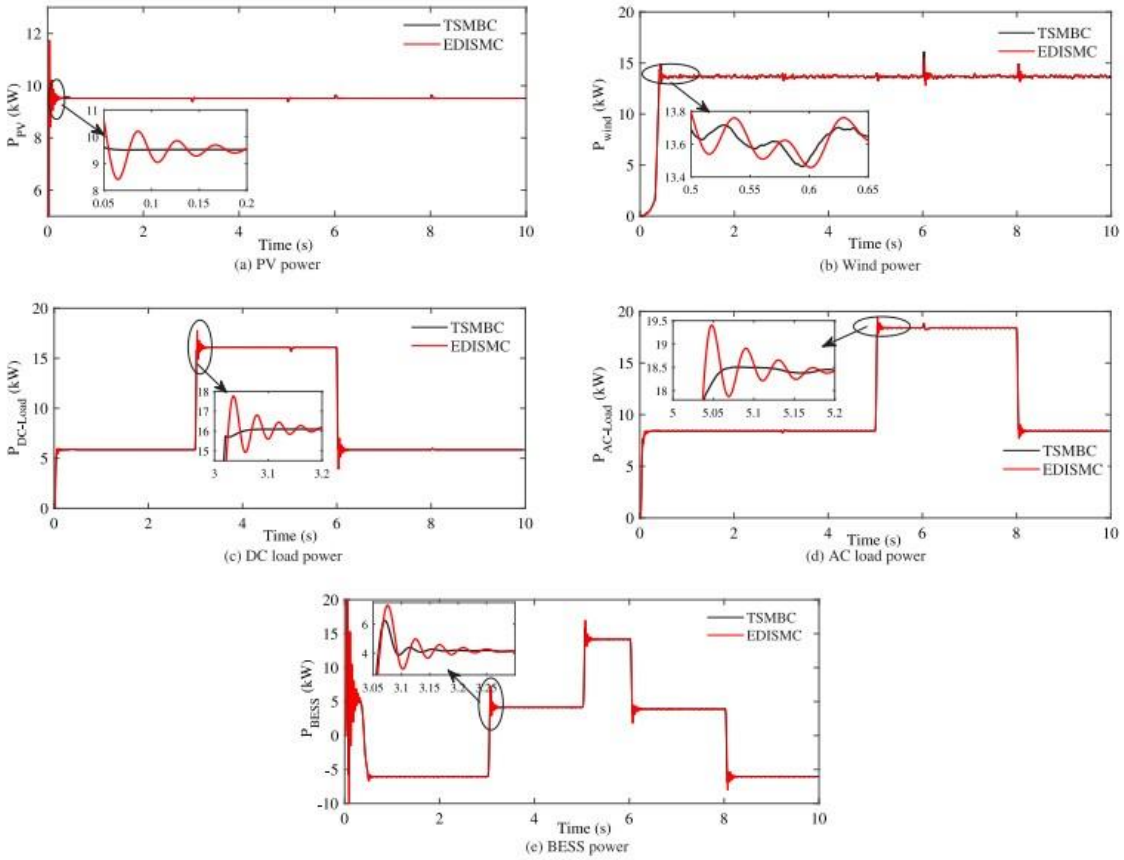


Figure 11: Dynamic stability of the solar PV system, wind generator system, DC load power, AC load power, and BESS power under case II.

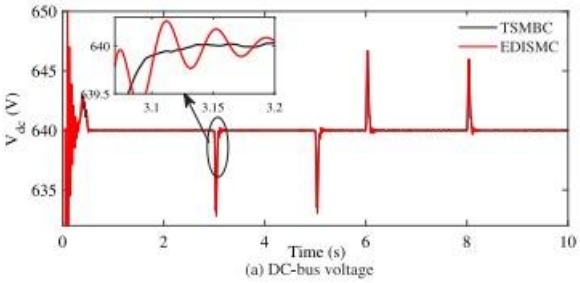


Figure 12: Dynamic stability of the DC bus under case II.

Table 10: Power flows of Figure 11.

Power flows	After transient t = 3 s	After transient t = 5 s	After transient t = 6 s	After transient t = 8 s
P_{PV} (KW)	9.50	9.50	9.50	9.50
P_{wind} (KW)	13.66	13.66	13.66	13.66
$P_{DC-load}$ (KW)	16.09	16.09	5.852	5.852
$P_{AC-load}$ (KW)	18.50	18.50	18.50	8.41
P_{BESS} (KW)	4.153	14.25	3.95	-6.08

As seen in Figure11(c), the DC load demand suddenly rises from 5.852 kW to 16.090 kW between t = 3 s and 6 s, while all other parameters stay constant. The power profiles in Figure 9 make it evident that the BESS releases energy to preserve power balance (see Figure11(e)). The DC bus and power responses following post-transient steady state are displayed in Figures. 9 and 10, which illustrate the value of the suggested controller. At t = 5 s, the AC load power increases from 8.410 kW to 18.500 kW, and the power profiles of the other units continue to run similarly to the previous phase until t = 6 s. Because the total output is less than full demand in this case, the BVSC will send 18.500 kW from the DC-side to the AC-side, and the BESS will transition to the discharge phase to maintain power balance. During these transients, the voltage at the DC bus encounters significant disturbances compared to the preceding case study. However, the suggested composite controller can manage and stabilise the bus voltage when the effects of this disturbance are contrasted with the current controller.

At this point, or t = 6 s, as shown in Figure11(c), the DC load drops from 16.090 kW to 5.852 kW, with all other parameters staying constant. This process is repeated until t = 8 s. In this instance, the BVSC will export additional power from the microgrid's DC component in order to meet the demand for the AC load. However, as illustrated in Figure11(e), the battery will produce the necessary energy to maintain the power balance because the overall output is less than the microgrid's demand. Ultimately, at t = 8 s, the AC load demand shifts from 18.500 kW to 8.410 kW, but the DC load demand and the electricity generated by wind and PV remain unchanged from the previous phase. This activity continues until t = 10 s. At this point, the BESS will release less energy than at the previous level, and the BVSC will move 8.410 kW of power from the DC-side to the AC side. As shown in Figure11, the output power's dynamic response for different units is least affected by the minor disturbance. Nevertheless, Figure 12 shows that this disruption has minimal impact on the DC bus voltage. It is evident that this disturbance significantly affects stability as compared to normal settings. To help with comprehension, Table 10 provides a comprehensive summary of the power flow shown in Figure11. Although the planned controller has a faster transient response, fewer overshoots, and a quicker settling time than the current controller, it is clear from the simulation results that both controllers maintain power balancing and maintain the correct DC bus voltage at all times. The quantitative results for both scenarios are shown in Tables 4 through 9. It is clear from these data that the suggested controller performs better than the current controller.

5.4. Discussion

A performance comparison between the proposed TSMBC and EDISMC was carried out across multiple system components. The quantitative analysis highlights that the proposed controller consistently outperformed the existing one, especially in terms of overshoot reduction and settling time improvement.

Table 11: Overall Performance Comparison Between TSMBC and EDISMC

Microgrid Component	Metric	EDISMC (Existing)	TSMBC (Proposed)	Improvement
PV Unit	Overshoot (%)	2.90–9.22	0	100% reduction
	Settling Time (ms)	250	2.5	99% faster
PMSG Unit	Overshoot (%)	6.90	0	100% reduction
	Settling Time (ms)	200	100	50% faster
DC Load	Overshoot (%)	Up to 31.64	0	100% reduction
	Settling Time (ms)	Up to 210	As low as 20	Up to 90% faster
AC Load	Overshoot (%)	Up to 16.76	0	100% reduction
	Settling Time (ms)	200	As low as 2.55	Up to 98% faster
BESS	Overshoot (%)	Up to 82.92	Much lower	70–95% reduction
DC Bus Voltage	Overshoot (%)	~0.03	0	100% reduction
	Settling Time (ms)	Up to 260	As low as 60	77% faster

The performance data in Table 11 clearly demonstrate the effectiveness of the proposed TSMBC controller over the existing EDISMC method. In the case of the PV unit, the TSMBC reduced overshoot from 2.90–9.22% to 0%, with a significant improvement in settling time from 250 ms to just 2.5 ms, indicating a 99% faster response. Similarly, for the PMSG unit, the overshoot was completely eliminated and the settling time improved by 50%, decreasing from 200 ms to 100 ms.

In DC load conditions, where EDISMC showed overshoot values of up to 31.64%, TSMBC again reduced overshoot to zero and improved settling time from as high as 210 ms to as low as 20 ms, offering up to 90% faster stabilization. The AC load performance also showed zero overshoot under TSMBC compared to up to 16.76% with EDISMC, and settling time was improved from 200 ms to a range between 2.55 ms and 60 ms—up to 98% faster.

In the BESS unit, although EDISMC exhibited overshoot of up to 82.92%, the proposed controller significantly lowered it, achieving a 70–95% reduction. For the DC bus voltage, TSMBC maintained perfect performance with zero overshoot, compared to slight overshoot in EDISMC (~0.03%), and also improved the settling time from as high as 260 ms to as low as 60ms.

These consistent improvements across all components highlight TSMBC's ability to provide faster, more stable responses with minimal overshoot, making it highly suitable for maintaining dynamic stability in hybrid AC/DC microgrid environments.

Chapter 6
Conclusion

To ensure the dynamic stability and efficient operation of a hybrid AC/DC microgrid, this thesis proposed a composite controller, integrating backstepping controller. The controller design is validated through rigorous Lyapunov stability analysis and tested under various transient and disturbance scenarios using MATLAB/Simulink simulations. The control objective is to achieve stable DC bus voltage regulation and robust power-sharing among different components including solar PV, PMSG, BESS, AC/DC loads, electrolyzer, PEM fuel cell and hydrogen storage systems.

Case 1: Controller performance under variation of the generated power

In Case I, the controller performance is evaluated under variations in generated power due to changes in solar irradiance and wind speed. The proposed TSMBC controller showed significantly better handling of power flow and DC bus voltage during transients compared to the existing EDISMC controller.

Quantitatively, the proposed controller achieves up to 100% reduction in overshoot and up to 99% faster settling time across key units like PV, PMSG, AC/DC loads, BESS, and DC bus voltage. Specifically, in the PV unit (Table 4), the overshoot was reduced from up to 9.22% to 0%, and settling time improved from 250 ms to 2.5 ms. Similar trends were observed in other components: overshoot in AC loads dropped from 16.76% to 0%, and DC load settling time improved from 210 ms to as low as 20 ms. These improvements were validated through Figures 9 and 10, where the TSMBC controller maintained smoother voltage profiles and faster responses under fluctuating power conditions.

Case 2: Controller performance under variation of the load demand

In Case II, the performance of the proposed controller is assessed under varying load demand conditions, including sudden increases and decreases in both DC and AC loads. The TSMBC controller effectively managed these transients—such as the DC load rising from 5.852 kW to 16.090 kW and the AC load from 8.410 kW to 18.500 kW—while maintaining overall power balance and voltage stability. The DC bus voltage, which experienced greater fluctuations during these disturbances, was quickly stabilized by the proposed controller compared to the existing EDISMC.

As reflected in Tables 4 to 9 and illustrated in Figures 11 and 12, the TSMBC controller maintained similar performance under load variations as in the previous case, with complete overshoot elimination and significantly faster settling times across all major units. These results further confirm the controller's robustness and adaptability in handling dynamic load conditions within hybrid AC/DC microgrid environments.

Future Work

Although the proposed controller performs well in simulation, a few challenges remain for practical implementation:

- **Gain tuning complexity:** Optimal parameter tuning is critical for real-time performance. Incorporating machine learning techniques could enable automatic tuning of gains.
- **Adaptive robustness**: The current design assumes fixed system parameters. In the future, a robust adaptive control framework should be developed to handle parametric uncertainties and unmodeled dynamics.
- **Experimental validation**: The next step should include hardware-in-the-loop testing or implementation on a real-time testbed to validate performance beyond simulations.

This work lays a strong foundation for intelligent and resilient microgrid control. Continued development in this area will support broader renewable energy adoption and pave the way for next-generation, low-carbon energy infrastructure.

References

1. Zehra SS, Rahman AU, Armghan H, Ahmad I, Ammara U. Artificial intelligence-based nonlinear control of renewable energies and storage system in a DC microgrid. ISA Trans 2022;121:217–31.
2. Pathak PK, Yadav AK, Padmanaban S, Alvi P, Kamwa I. Fuel cell-based topologies and multi-input DC–DC power converters for hybrid electric vehicles: A comprehensive review. IET Gener, Transm Distribution 2022;16(11):2111–39.
3. Wu D, Tang F, Dragicevic T, Vasquez JC, Guerrero JM. A control architecture to coordinate renewable energy sources and energy storage systems in islanded microgrids. IEEE Trans Smart Grid 2014;6(3):1156–66.
4. Wang Z, Chen B, Wang J, et al. Decentralized energy management system for networked microgrids in grid-connected and islanded modes. IEEE Trans Smart Grid 2015;7(2):1097–105.
5. Ahmed M, Meegahapola LG, Datta M, Vahidnia A. A novel hybrid AC/DC microgrid architecture with a central energy storage system. IEEE Trans Power Deliv 2021.
6. Sepehrzad R, Moridi AR, Hassanzadeh ME, Seifi AR. Intelligent energy management and multi-objective power distribution control in hybrid micro-grids based on the advanced fuzzy-PSO method. ISA Trans 2021;112:199–213.
7. Amiri H, Markadeh GA, Dehkordi NM, Blaabjerg F. Fully decentralized robust backstepping voltage control of photovoltaic systems for DC islanded microgrids based on disturbance observer method. ISA Trans 2020;101:471–81.
8. Roy TK, Mahmud MA, Oo AMT, Haque ME, Muttaqi KM, Mendis N. Nonlinear adaptive backstepping controller design for islanded DC microgrids. IEEE Trans Ind Appl 2018;54(3):2857–73.
9. Heidary J, Gheisarnejad M, Khooban MH. Stability enhancement and energy management of AC-DC microgrid based on active disturbance rejection control. Electr Power Syst Res 2023;217:109105.
10. Sedhom BE, El-Saadawi MM, Elhosseini MA, Saeed MA, Abd-Raboh EE. A harmony search-based H-infinity control method for islanded microgrid. ISA Trans 2020;99:252–69.
11. Liu X, Wang P, Loh PC. A hybrid AC/DC microgrid and its coordination control. IEEE Trans Smart Grid 2011;2(2):278–86.
12. Manbachi M, Ordonez M. Intelligent agent-based energy management system for islanded AC–DC microgrids. IEEE Trans Ind Inf 2019;16(7):4603–14.
13. Loh PC, Li D, Chai YK, Blaabjerg F. Hybrid AC–DC microgrids with energy storages and progressive energy flow tuning. IEEE Trans Power Electron 2012;28(4):1533–43.
14. Menaga D, Sankaranarayanan V. A novel nonlinear sliding mode controller for a single stage grid-connected photovoltaic system. ISA Trans 2020;107:329–39.
15. Senapati MK, Pradhan C, Samantaray SR, Nayak PK. Improved power management control strategy for renewable energy-based DC microgrid with energy storage integration. IET Gener, Transm Distribution 2019;13(6):838–49.
16. Chinchilla M, Arnaltes S, Burgos JC. Control of permanent-magnet generators applied to variable-speed wind-energy systems connected to the grid. IEEE Trans Energy Convers 2006;21(1):130–5.
17. Ackermann T. Wind power in power systems. Vol. 200, (5). Wiley New York; 2005.
18. Shan Y, Pan A, Liu H. A switching event-triggered resilient control scheme for primary and secondary levels in AC microgrids. ISA Trans 2022.
19. Melath G, Rangarajan S, Agarwal V. A novel control scheme for enhancing the transient performance of an islanded hybrid AC–DC microgrid. IEEE Trans Power Electron 2019;34(10):9644–54.

20. Ma T, Cintuglu MH, Mohammed OA. Control of a hybrid AC/DC microgrid involving energy storage and pulsed loads. IEEE Trans Ind Appl 2016;53(1):567–75.
21. Sowmmiya U, Govindarajan U. Control and power transfer operation of WRIG-based WECS in a hybrid AC/DC microgrid. IET Renew Power Gener 2017;12(3)
22. Pathak PK, Yadav AK, Shastri A, Alvi P. BWOA assisted PIDF-(1+ I) controller for intelligent load frequency management of standalone micro-grid. ISA Trans 2022.
23. Xia Y, Peng Y, Yang P, Yu M, Wei W. Distributed coordination control for multiple bidirectional power converters in a hybrid AC/DC microgrid. IEEE Trans Power Electron 2016;32(6):4949–59.
24. Wang C, Li X, Guo L, Li YW. A nonlinear-disturbance-observer-based DC-bus voltage control for a hybrid AC/DC microgrid. IEEE Trans Power Electron 2014;29(11):6162–77.
25. Loh PC, Li D, Chai YK, Blaabjerg F. Autonomous operation of hybrid microgrid with AC and DC subgrids. IEEE Trans Power Electron 2012;28(5):2214–23.
26. Wang J, Jin C, Wang P. A uniform control strategy for the interlinking converter in hierarchical controlled hybrid AC/DC microgrids. IEEE Trans Ind Electron 2017;65(8):6188–97.
27. Golsorkhi MS, Savaghebi M. A decentralized control strategy based on VI Droop for enhancing dynamics of autonomous hybrid AC/DC microgrids. IEEE Trans Power Electron 2021;36(8):9430–40.
28. Zhang Q, Zhuang X, Liu Y, Wang C, Guo H. A novel control strategy for mode seamless switching of PV converter in DC microgrid based on double integral
29. Martin AD, Cano J, Silva JFA, Vazquez JR. Backstepping control of smart grid-connected distributed photovoltaic power supplies for telecom equipment. IEEE Trans Energy Convers 2015;30(4):1496–504.
30. Bahrami, S., Mousavi, S.S., Shafiee-Rad, M.: Decentralized adaptive nonlinear controller for voltage regulation of output-constrained DC microgrids with ZIP loads. IEEE Trans. Power Syst. 39(5), 6210–6221 (2024)
31. Jiang, W., Wang, Z., Li, X., Ma, R., Huang, S., Dong, C., Wu, X.: Largesignal stabilization of interleaved multilevel boost converter interfaced high power DC microgrid using an adaptive observer based nonlinear control scheme. IEEE Trans. Power Electron. 39(7), 8242–8253 (2024)
32. Tatari, F.R., Banejad, M., Kalat, A.A.: A move blocking based direct voltage model predictive control to enhance the dynamic performance of DC microgrids containing constant power loads. IET Renewable Power Gener. 17(13), 3340–3354 (2023)
33. Aghdam, M.M., Li, L., Zhu, J.: Comprehensive study of finite control set model predictive control algorithms for power converter control in microgrids. IET Smart Grid 3(1), 1–10 (2020)
34. Zhao, Z., Xu, J., Guo, J., Ni, Q., Chen, B., Lei, L.L.: Robust energy management for multi-microgrids based on distributed dynamic tube model predictive control. IEEE Trans. Smart Grid 15(1), 203–217 (2023)
35. Dragicevi ˇ c, T., Novak, M.: Weighting factor design in model predic- ´ tive control of power electronic converters: an artificial neural network approach. IEEE Trans. Ind. Electron. 66(11), 8870–8880 (2018)
36. Mahmud, M.A., Roy, T.K., Islam, S.N., Saha, S., Haque, M.E.: Nonlinear decentralized feedback linearizing controller design for islanded DC microgrids. Electr. Power Compon. Syst. 45(16), 1747–1761 (2017)
37. Mahmud, M.A., Roy, T.K., Saha, S., Haque, M.E., Pota, H.R.: Robust nonlinear adaptive feedback linearizing decentralized controller design for islanded DC microgrids. IEEE Trans. Ind. Appl. 55(5), 5343–5352 (2019)
38. Armghan, H., Yang, M., Wang, M., Ali, N., Armghan, A.: Nonlinear integral backstepping based control of a DC microgrid with renewable generation and energy storage systems. Int. J. Electr. Power Energy Syst. 117, 105613 (2020)
39. Roy, T.K., Mahmud, M.A.: Dynamic stability analysis of hybrid islanded DC microgrids using a nonlinear backstepping approach. IEEE Syst. J. 12(4), 3120–3130 (2017)

40. Roy, T.K., Mahmud, M., Oo, A.M.: Operations of DC microgrids in coordination with AC grids based on nonlinear backstepping controllers. In: 2018 IEEE Power & Energy Society General Meeting (PESGM), pp. 1–5. IEEE, Piscataway, NJ (2018)
41. Roy, T.K., Mahmud, M.A., Oo, A.M.T, Haque, M.E., Muttaqi, K.M., Mendis, N.: Nonlinear adaptive backstepping controller design for islanded DC microgrids. IEEE Trans. Ind. Appl. 54(3), 2857–2873 (2018)
42. Li, X., Wang, M., Jiang, W., Dong, C., Xu, Z., Wu, X.: An autonomous finite-time backstepping control for decentralized automatic power sharing of hybrid energy storage systems in DC microgrids. IEEE Trans. Smart Grid 15(4), 3348–3360 (2024)
43. Dong, C., Jiang, W., Wang, Z., Jiang, F., Jia, H.: Unified multimode modelling, stability analysis, and reinforced sliding-mode design of high-order buck/boost DC–DC converters for DC energy systems. IET Energy Syst. Integr. 3(4), 397–412 (2021)
44. Mosayebi, M., Gheisarnejad, M., Khooban, M.H.: An intelligent sliding mode control for stabilization of parallel converters feeding CPLs in DC-microgrid. IET Power Electron. 15(14), 1596–1606 (2022)
45. Maged, N.A., Hasanien, H.M., Ebrahim, E.A., Tostado-Véliz, M., Jurado, F.: Optimal super twisting sliding mode control strategy for performance improvement of islanded microgrids: validation and real-time study. Int. J. Electr. Power Energy Syst. 157, 109849 (2024)
46. Thomas, T., Mishra, M.K., Kumar, C., Liserre, M.: Control of a PV-wind based DC microgrid with hybrid energy storage system using Lyapunov approach and sliding mode control. IEEE Trans. Ind. Appl. 60(2), 3746– 3758 (2024)
47. Wang, B., Li, Z., Fan, H., Wan, X., Xian, L., Zhang, M., Xu, Q.: Higher order sliding mode observer based fast composite backstepping control for HESS in DC microgrids. IEEE Trans. Sustainable Energy 15(3), 1627– 1639 (2024)
48. Ullah, Q., Busarello, T.D.C, Brandao, D.I., Simões, M.G.: Design and performance evaluation of SMC-based DC–DC converters for microgrid applications. Energies 16(10), 4212 (2023)
49. Ranganathan, S., Sathi, R.R.: Design and analysis of fast response sliding mode controller for quadratic boost converter based hybrid PV/wind system in DC micro-grid. J. Electr. Eng. Technol. 16(5), 2561–2571 (2021)
50. Teng, Q., Liu, X., Mai, H., Xing, K., Li, M., Ma, X., Wang, Y.: Nonsingular fast terminal sliding mode control for two-stage converters of AC island photovoltaic microgrid. Appl. Energy 352, 122023 (2023)
51. Bagheri, A., Jabbari, A., Mobayen, S.: An intelligent ABC-based terminal sliding mode controller for load-frequency control of islanded micro-grids. Sustainable Cities Soc. 64, 102544 (2021)
52. Bagheri, A., Jabbari, A., Mobayen, S.: An intelligent ABC-based terminal sliding mode controller for load-frequency control of islanded micro-grids. Sustainable Cities Soc. 64, 102544 (2021)
53. Roy, T.K., Oo, A.M.T, Ghosh, S.K.: Designing a high-order sliding mode controller for photovoltaic-and battery energy storage system-based DC microgrids with ANN-MPPT. Energies 17(2), 532 (2024)
54. Ghosh, S.K., Roy, T.K., Pramanik, M.A.H, Mahmud, M.A.: A nonlinear double-integral sliding mode controller design for hybrid energy storage systems and solar photovoltaic units to enhance the power management in DC microgrids. IET Gener. Transm. Distrib. 16(11), 2228–2241 (2022)
55. Thomas, T., Mishra, M.K., Kumar, C., Liserre, M.: Control of a PV-wind based DC microgrid with hybrid energy storage system using Lyapunov approach and sliding mode control. IEEE Trans. Ind. Appl. 60(2), 3746– 3758 (2024)
56. Thomas, T., Mishra, M.K., Kumar, C., Liserre, M.: Control of a PV-wind based DC microgrid with hybrid energy storage system using Lyapunov approach and sliding mode control. IEEE Trans. Ind. Appl. 60(2), 3746– 3758 (2024)
57. Ghosh, S.K., Roy, T.K., Pramanik, M.A.H, Mahmud, M.A.: A nonlinear double-integral sliding mode controller design for hybrid energy storage systems and solar photovoltaic units to enhance the power management in DC microgrids. IET Gener. Transm. Distrib. 16(11), 2228–2241 (2022)

58. Roy, T.K., Pramanik, M.A.H., Ghosh, S.K.: Design of an integral terminalbased sliding mode controller for PV and BESS-based DC microgrids. Energy Nexus 7, 100130 (2022)
59. Yeasmin, S., Roy, T.K., Ghosh, S.K.: Design of robust integral terminal sliding mode controllers with exponential reaching laws for solar PV and BESS-based DC microgrids with uncertainties. Sustainability 14(13), 7802 (2022)
60. Islam, M.S., Bushra, I.J., Roy, T.K., Ghosh, S.K.: Design of global integral terminal sliding mode controller with exponential reaching law for solar PV and BESS–based DC microgrids. In: 2024 3rd International Conference on Advancement in Electrical and Electronic Engineering (ICAEEE), pp. 1–6. IEEE, Piscataway, NJ (2024)
61. Korompili, A., Monti, A.: Review of modern control technologies for voltage regulation in DC/DC converters of DC microgrids. Energies 16(12), 4563 (2023).
62. Prasad, E.N., Sahani, M., Dash, P.: A new adaptive integral back stepping fractional order sliding mode control approach for PV and wind with battery system based DC microgrid. Sustainable Energy Technol. Assess. 52, 102261 (2022).
63. Roy, T.K., Ghosh, S.K., Saha, S.: Stability enhancement of battery energy storage and renewable energy-based hybrid AC/DC microgrids using terminal sliding mode backstepping control approaches. ISA Trans. 142, 40–56 (2023).
64. Roy, T.K., Ghosh, S.K., Saha, S.: Robust backstepping global integral terminal sliding mode controller to enhance dynamic stability of hybrid AC/DC microgrids. Prot. Control Mod. Power Syst. 8(1), 8 (2023).
65. Muktiadji, R.F., Ramli, M.A.: Bouchekara, H.R., Milyani, A.H., Rawa, M., Seedahmed, M.M., Budiman, F.N.: Control of boost converter using observer-based backstepping sliding mode control for DC microgrid. Front. Energy Res. 10, 828978 (2022).
66. Chabukswar, A., Wandhare, R.: Modified back-stepping sliding mode controller with robust observer-less disturbance rejection for DC microgrid applications. IEEE Trans. Power Electron. 40(1), 451–466 (2024).
67.] Zhang Z, Fang J, Dong C, Jin C, Tang Y. Enhanced grid frequency and DC-link voltage regulation in hybrid AC/DC microgrids through bidirectional virtual inertia support. IEEE Trans Ind Electron July 2023;70(7):6931–40.
68.] Li C, Yang Y, Cao Y, Aleshina A, Xu J, Blaabjerg F. Grid inertia and damping support enabled by proposed virtual inductance control for grid-forming virtual synchronous generator. IEEE Trans Power Electron Jan. 2023;38(1):294–303.
69.] Zhong Q-C, Nguyen P-L, Ma Z, Sheng W. Self-synchronized synchronverters: inverters without a dedicated synchronization unit. IEEE Trans Power Electron Feb. 2014;29(2):6.
70.] Wang L, Fu X, Wong M-C. Operation and control of a hybrid coupled interlinking converter for hybrid AC/low voltage DC microgrids. IEEE Trans Ind Electron Aug. 2021;68(8):7104–1.
71. Augustine S, Mishra MK, Lakshminarasamma N. Adaptive droop control strategy for load sharing and circulating current minimization in low-voltage standalone DC microgrid. IEEE Trans Sustain Energy Jan. 2015;6(1):132–41.
72. Qi G, Chen A, Chen J. Improved control strategy of interlinking converters with synchronous generator characteristic in islanded hybrid AC/DC microgrid. CPSS Trans Power Electron Appl 2017;2(2):149–58.
73. Li X, Guo Li, Li Y, Guo Z, Hong C, Zhang Ye, et al. A unified control for the DC–AC interlinking converters in hybrid AC/DC microgrids. IEEE Trans Smart Grid 2018;9 (6):6540–53.
74. Augustine S, Mishra MK, Lakshminarasamma N. Adaptive droop control strategy for load sharing and circulating current minimization in low-voltage standalone DC microgrid. IEEE Trans Sustain Energy Jan. 2015;6(1):132–41.
75. Lu X, Guerrero JM, Sun K, Vasquez JC. An improved droop control method for DC microgrids based on low bandwidth communication with DC bus voltage restoration and enhanced current sharing accuracy. IEEE Trans Power Electron Apr. 2014;29(4):1800–12.

76. Xiao J, Wang P, Setyawan L. Multilevel energy management system for hybridization of energy storages in DC microgrids. IEEE Trans Smart Grid Mar. 2016;7(2):847–56.
77. Morstyn T, Hredzak B, Demetriades GD, Agelidis VG. Unified distributed control for DC microgrid operating modes. IEEE Trans Power Syst Jan. 2016;31(1):802–12.
78. Samanta S, Mishra JP, Roy BK. Virtual DC machine: An inertia emulation and control technique for a bidirectional DC–DC converter in a DC microgrid. IET Elect Power Appl Jul. 2018;12(6):874–84.
79. Fang J, Tang Y, Li H, Li X. A battery/ultracapacitor hybrid energy storage system for implementing the power management of virtual synchronous generators. IEEE Trans Power Electron 2018;33(4):2820–4.
80. Baghaee HR, Mirsalim M, Gharehpetian GB, Talebi HA. A decentralized power management and sliding mode control strategy for hybrid AC/DC microgrids including renewable energy resources. IEEE Trans Ind Inform 2017.